

A carbon cycle coupled climate model of Neoproterozoic glaciation: Explicit carbon cycle with stochastic perturbations

Yonggang Liu¹ and W. Richard Peltier¹

Received 29 September 2010; accepted 1 November 2010; published 28 January 2011.

[1] It has been suggested that a negative climate feedback may have operated during the Neoproterozoic Era as a consequence of the existence of a massive oceanic pool of dissolved organic carbon (DOC). As climate cooled so as to induce intense glaciation, the drawdown of oxygen into the Neoproterozoic ocean would have been enhanced because of the temperature dependence of the solubility of oxygen in seawater. Such increasing ventilation would have enhanced DOC remineralization, thus increasing the content of dissolved inorganic carbon (DIC) in the ocean. CO₂ concentration in the atmosphere increases rapidly with DIC, thereby inhibiting further climate cooling. The model employed to illustrate the resulting climate dynamical behavior was an idealized one in which stochastic influence was assumed to be absent. However, such influence is expected to exist due to the action of processes that are not explicitly included in the model. Furthermore, the paleogeography assumed for the purpose of the published analyses was more appropriate to the Marinoan glaciation than to the earlier Sturtian event. In this paper, we fully investigate the stability of the system represented by the carbon cycle coupled climate model for both the Marinoan and Sturtian continental configurations and in the presence of stochastic perturbations. It is found that the hysteresis predicted by the ice sheet coupled model is sensitive to both continental configuration and to the strength of the negative feedback which arises due to carbon cycle coupling. Nevertheless, the very low frequency cyclic glaciation process predicted by the initial version of the model is found to persist in the presence of noise of significant amplitude. However, this cyclic behavior may be arrested entirely if the glaciation process were to result in insufficient alkalinity being delivered to the ocean basins. In this case the system would be expected to execute only a single excursion into and escape from the glacial state.

Citation: Liu, Y., and W. R. Peltier (2011), A carbon cycle coupled climate model of Neoproterozoic glaciation: Explicit carbon cycle with stochastic perturbations, *J. Geophys. Res.*, 116, D02125, doi:10.1029/2010JD015128.

1. Introduction

[2] The debate concerning the nature of Neoproterozoic glacial events has come to be widely joined, not only from the geological perspectives of sedimentology [Allen and Etienne, 2008; Allen *et al.*, 2004; Le Guerroué *et al.*, 2006; Leather *et al.*, 2002] and geochronology [Condon *et al.*, 2005] but also from the perspectives of paleomagnetism [Evans, 2006; Font *et al.*, 2005; Kirschvink, 1992; Li, 2000; Sohl *et al.*, 1999] and global tectonics [Li *et al.*, 2004, 2008; Trindade and Macouin, 2007] as well as that of a priori climate system modeling [Chandler and Sohl, 2000; Crowley *et al.*, 2001; Hyde *et al.*, 2000; Le Hir *et al.*, 2007; Peltier *et al.*, 2004, 2007; Pierrehumbert, 2004, 2005; Poulsen, 2003; Poulsen and Jacob, 2004]. The focus of this debate has been upon the question as to whether or not cryogenian

glacial events may have been of “snowball” form, the “snowball” appellation being that originally suggested by Kirschvink [1992] to describe a climate state in which the continents were covered by thick ice sheets and the oceans by a continuous veneer of thick sea ice. In the present paper we will refer to such fully glaciated states as “hard snowball” states. It was first suggested by Hyde *et al.* [2000] that an alternative interpretation of the admittedly intense Neoproterozoic glaciations may be at least equally plausible, namely that these glaciations, although extreme, may have been such that, although the continents were indeed covered by thick ice sheets, the oceans may not have been fully covered by sea ice; rather, a significant area of open water may have persisted at the equator. The latter solutions were originally termed “slushball” states in the criticism of this alternative view offered by Schrag and Hoffman [2001].

[3] In the recent paper by Peltier *et al.* [2007], a further analysis of Neoproterozoic glacial events was presented in which the climate model employed by Hyde *et al.* [2000], namely that developed previously by DeBlonde and Peltier

¹Department of Physics, University of Toronto, Toronto, Ontario, Canada.

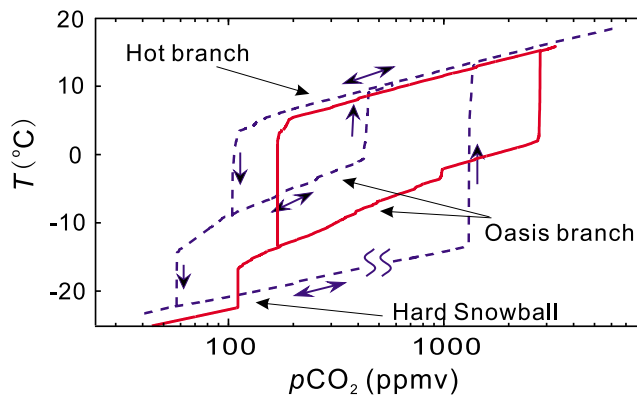


Figure 1. Hysteresis loop of steady state solutions for both the 570 Ma (blue dashed line) and 720 Ma continental configurations of the climate model in the absence of carbon cycle coupling (red solid line). This is reproduced from Figure 5e of Liu and Peltier [2010].

[1993], was augmented by coupling the original model of surface climate in which continental ice sheet dynamics was treated explicitly to an active model of the carbon cycle. Whereas the original model had been employed primarily to compute steady state solutions for surface climate given an assumed level of atmospheric carbon dioxide concentration and an appropriate value of the solar constant for Neoproterozoic time, when coupled to the carbon cycle the new model was shown to support an entirely new class of solutions. With the paleogeography fixed to a facsimile of that appropriate to the Marinoan glaciation, the addition of active carbon cycle coupling in the enhanced model of Peltier *et al.* [2007] endowed the model system with active dynamical behavior. The essence of this dynamical behavior lay in the fact that the earlier version of the model exhibited hysteresis in the state-space of model solutions defined by the two variables of mean surface temperature and atmospheric carbon dioxide concentration [Crowley *et al.*, 2001]. Although at high carbon dioxide concentrations the steady state solutions were such that the continents were entirely free of ice sheets and the oceans of sea ice and at very low carbon dioxide concentrations only the “hard snowball” Earth solution was present, in an intermediate range of carbon dioxide concentrations multiple equilibria existed. Which of these equilibria was physically realized depended upon the conditions in which the model was initialized. The “slushball” solution was shown to exist as a physically realizable steady state solution in this intermediate range of atmospheric carbon dioxide concentration. Such solutions were characterized by heavily glaciated continents but by sea ice that remained restricted to the polar regions.

[4] With the addition of coupling to the carbon cycle the model was shown to be endowed with intrinsically dynamical behavior during which the system simply cycled the hysteresis loop of steady state solutions that characterized the state space of the model in the absence of this coupling. In the language of “dynamical systems” the hysteresis loop acted as an “attactor” of carbon cycle coupled climate dynamics. The key assumption upon which this version of the model was constructed involved the implementation of a two box model of the carbon cycle that had

been suggested as appropriate for the Neoproterozoic by Rothman *et al.* [2003]. These authors had argued that the carbon cycle during this period was rather special. Whereas during Phanerozoic time the carbon cycle had apparently operated in equilibrium (or equivalently in a steady state), as demonstrated by the fact that the difference between $\delta^{13}\text{C}_{\text{carbonate}}$ and $\delta^{13}\text{C}_{\text{organic}}$ was approximately time invariant, during the Neoproterozoic this relationship ceased to hold. The authors demonstrated that such out-of-equilibrium behavior could be understood if it were assumed that the mass of organic carbon in the Neoproterozoic ocean was greatly in excess of the inorganic mass. In the work of Peltier *et al.* [2007] this model of the carbon cycle was coupled to a similar ice sheet coupled climate model as that employed by Hyde *et al.* [2000]. One further enhancement of the model structure introduced was to employ the full thermomechanical version of the University of Toronto Glacial Systems Model (UofT GSM) [e.g., see Tarasov and Peltier, 1999] to represent continental ice sheet dynamics rather than the earlier isothermal model of DeBlonde and Peltier [1993]. The coupling between the climate and carbon cycle components of the model was assumed to operate through the atmospheric concentrations of oxygen and carbon dioxide. As temperature falls, ocean ventilation increases as a consequence of the temperature dependence of the solubility of oxygen in seawater [García and Gordon, 1992]. In the presence of increasing oxygen concentration in the oceans, the rate of respiration of the massive pool of dissolved organic carbon in the oceans increases. This increases the amount of dissolved carbon dioxide in the oceans. On the basis of the further assumption that the oceans are saturated with respect to carbonate one may compute the fraction of the excess ocean carbon dioxide that would be partitioned into the atmosphere [Kump and Arthur, 1999]. It is this set of interactions that allows the carbon cycle coupled version of the climate model to support a nonlinear auto-oscillation in which cyclic glaciation and deglaciation cycles continue endlessly when the single control parameter of the model is fixed to lie within a certain range of values. The glacial interglacial timescale delivered by the model is such that it lies well within the range of cycle times allowed by the geological constraints.

[5] The model of Peltier *et al.* [2007] has recently been debated in the sequence of comments and replies recorded by Hoffman *et al.* [2008], Goddard and Donnadieu [2008], and Peltier and Liu [2008]. Issues raised in this sequence of exchanges warrant further discussion and it is the purpose of this paper to more fully elaborate on several of the more important. In an earlier paper [Liu and Peltier, 2010] the issue of the paleocontinental reconstruction employed in the coupled model analysis was addressed in some detail. There it was shown that the existence of the hysteresis loop in the state space of steady solutions when carbon cycle coupling was not included, which is crucial for the existence of the active glacial cycles described by Peltier *et al.* [2007], persists over a broad range of paleogeographies that includes the most recent reconstruction for Sturtian time in which a significant continental mass exists in the equatorial region (see Figure 1 where the Sturtian hysteresis loop of Liu and Peltier [2010] is reproduced together with that for the Marinoan-like event from Peltier *et al.* [2007]).

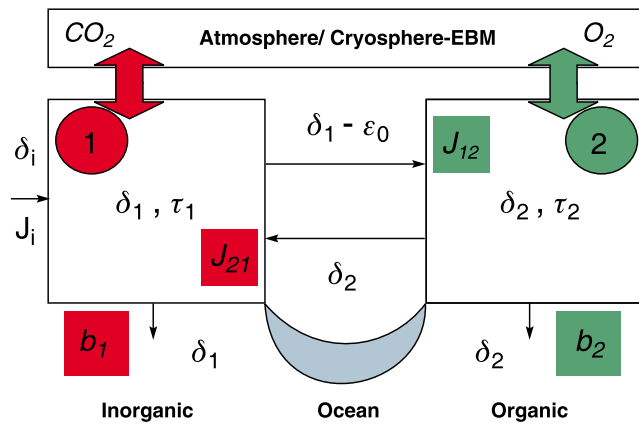


Figure 2. A schematic diagram of the carbon cycle coupled climate model that is employed for the purpose of the analyses in this paper. The variables $\delta_{1,2}$ and $\tau_{1,2}$ are the isotopic compositions and residence times for the inorganic and organic carbon reservoirs, respectively. Here δ_i is the input into the inorganic reservoir from, for example, volcanic outgassing and ε_0 is the isotopic fractionation that occurs in photosynthesis during which inorganic carbon is converted into organic carbon. Fluxes into and out of the two reservoirs are represented by the arrows. Output from the two reservoirs occurs directly by burial fluxes b_1 and b_2 as well as by exchanges between them. Crucial to the success of our coupled model of carbon-cycle-climate evolution are the fluxes of O_2 and CO_2 between the atmosphere and ocean components of the model.

[6] It was also suggested by *Hoffman et al.* [2008] that since our model contains neither sources nor sinks of atmospheric carbon dioxide it would not be robust in the presence of such additional dynamical processes and that the dynamical behavior it delivers would not persist in the presence of noise. In fact these two issues are closely linked. As explained by *Peltier and Liu* [2008], it was assumed in the preliminary analyses of *Peltier et al.* [2007] that the additional source of atmospheric carbon dioxide due to volcanic outgassing is precisely balanced by the sink associated with calcium-magnesium silicate weathering of the continents. Since that source-sink couplet was assumed to be in balance, it was unnecessary to consider either. *Berner* [2004] has argued that this balance has been closely maintained throughout Phanerozoic time. That it could have remained precisely balanced during the Neoproterozoic is, of course, unrealistic. As pointed out by *Peltier and Liu* [2008], it is the degree of imbalance between the outgassing source and the weathering sink against which the dynamics in our carbon cycle coupled climate model would be obliged to compete. Because it is of course impossible for us, or anyone else, to know what the degree of imbalance might have been in this source-sink couplet, in the present paper we will treat it as a source of noise and will thereby address the two issues in a single sequence of new realizations of model behavior. The methods we will employ to perform the analysis of the model response in the presence of such stochastic perturbations is that recently employed by *Stastna and Peltier* [2007] in their analysis of

a series of simple box models of the thermohaline circulation of the oceans.

[7] In the new sequence of analyses reported herein we will also quantitatively address the further two issues raised by *Hoffman et al.* [2008] and *Goddéris and Donnadieu* [2008], which are both directly related to the partitioning of CO_2 between atmosphere and ocean. One of these concerns the direct impact of CO_2 solubility in the Neoproterozoic ocean relative to that of oxygen in response to the lowering of temperature, the other concerns the influence of ocean alkalinity. As we will argue herein, neither of these issues is expected to have a significant impact upon the negative feedback mechanism described by *Peltier et al.* [2007].

2. Model Description

[8] The model to be employed herein consists of three primary components: A global surface energy balance module, a 3-D thermomechanical ice sheet module and a Neoproterozoic carbon cycle module. The EBM and ice sheet model components have been reviewed in detail in our recent paper [*Liu and Peltier*, 2010]. The ice sheet component originated in papers by *DeBlonde and Peltier* [1990, 1991, 1993], *DeBlonde et al.* [1992], and [*Tarasov and Peltier*, 1997, 1999, 2002, 2003]. The energy balance climate model employed is based upon that of *North et al.* [1981] which was enhanced by the addition of a sea ice component by *DeBlonde et al.* [1992]. Only the carbon cycle model will be fully discussed herein. We will also discuss the methodology employed to introduce stochastic perturbations into the model.

2.1. Carbon Cycle Model

[9] The ocean carbon cycle model has been briefly summarized by *Peltier et al.* [2007] but will be described in detail here in order to clarify the nature of the modifications required to the two-box model of *Rothman et al.* [2003], on which our own model is based, in order to couple the carbon cycle to the other components of the climate system. The carbon cycle model is depicted schematically in Figure 2, which is based upon that in the work of *Peltier et al.* [2007], which is itself an extension of Figure 3 of *Rothman et al.* [2003]. Crucial for our purposes are the processes that mediate exchanges of O_2 and CO_2 between the ocean and the overlying atmosphere.

[10] The set of nonlinear ordinary differential equations describing the dynamics of the *Rothman et al.* [2003] model are as follows:

$$\dot{\delta}_1 = \frac{J_i}{M_1}(\delta_i - \delta_1) + \frac{J_{21}}{M_1}(\delta_2 - \delta_1) + \frac{J_{12}}{M_1}\varepsilon_0, \quad (1)$$

$$\dot{\delta}_2 = \frac{J_{12}}{M_2}(\delta_1 - \varepsilon_0 - \delta_2), \quad (2)$$

$$\dot{M}_1 = J_i + J_{21} - J_{12} - b_1, \quad (3)$$

$$\dot{M}_2 = J_{12} - J_{21} - b_2, \quad (4)$$

which describe the temporal evolution of both the masses and carbon isotopic properties of the two carbon reservoirs in terms of which the ocean carbon cycle is described. In these equations, δ_1 , M_1 , and δ_2 , M_2 are the $\delta^{13}\text{C}$ isotopic ratios and the masses of the dissolved inorganic carbon (DIC) and DOC reservoirs, respectively; J_i represents the input flux into the inorganic reservoir, primarily associated with volcanic outgassing; and δ_i is the characteristic $\delta^{13}\text{C}$ ratio associated with this input flux. The additional parameters b_1 and b_2 are readily seen from Figure 2 to be the burial fluxes of carbon from the inorganic and organic carbon reservoirs, respectively, into the sediments on the ocean floor. On long timescales a portion of this component of the sediment pile is returned to the mantle due to the subduction of oceanic lithosphere. The fluxes J_{12} and J_{21} are the exchange fluxes between the two reservoirs, due to photosynthetic and respiratory/oxidative processes respectively. Here ε_0 is the photosynthetic fractionation coefficient by which the isotopic ratio of the inorganic carbon is modified due to the preferential uptake of ^{12}C relative to ^{13}C in the photosynthetic production of organic matter.

[11] In the work of *Rothman et al.* [2003], it was suggested that the carbon cycle was most probably operating in equilibrium during Phanerozoic time, in accord with the *Berner* [2004] analysis, whereas during the prior Neoproterozoic period, out of equilibrium behavior might have arisen as a consequence of the existence of a massive organic carbon reservoir, the mass of which was greatly in excess of that of the inorganic reservoir. In order to investigate the nature of the dynamical processes that would occur under such circumstances we may investigate the evolution of perturbations to an assumed equilibrium state described by the steady state solutions of equations (1)–(4). Such an equilibrium state is characterized by the following relations:

$$J_{12e} + b_{1e} \equiv J_{ie} + J_{21e} \equiv J_{1e}, \quad (5)$$

$$J_{21e} + b_{2e} \equiv J_{12e} \equiv J_{2e}, \quad (6)$$

in which J_{1e} and J_{2e} are defined so as to represent the TOTAL mass fluxes into and out of the inorganic and organic reservoirs, respectively, under steady state conditions. The residence time constants indicated on the box diagram in Figure 2 are defined at steady state to be

$$\tau_1 = M_{1e}/J_{1e}, \quad (7)$$

$$\tau_2 = M_{2e}/J_{2e}. \quad (8)$$

At steady state, several additional quantities that are useful in representing the steady state solutions of the *Rothman et al.* [2003] model are the normalized photosynthetic flux, ϕ_{12} , the organic fraction of the total burial flux, f , and the ratio of the residence times, μ . These quantities are defined as:

$$\phi_{12} = J_{12e}/J_{1e} \quad (9)$$

$$f = b_{2e}/(b_{1e} + b_{2e}) \quad (10)$$

$$\mu = \tau_1/\tau_2 \quad (11)$$

The steady state solutions of the model may be defined in terms of these quantities. The mass of the organic carbon reservoir and the fluxes connecting the reservoirs to one another and to the external environment at equilibrium are described through M_1 , τ_1 , ϕ , f and μ as follows:

$$M_{2e} = \frac{\phi_{12}M_{1e}}{\mu}, \quad (12)$$

$$J_{ie} = \frac{M_{1e}(1 - \phi_{12})}{\tau_1(1 - f)} \quad (13)$$

$$J_{12e} = \frac{M_{1e}\phi_{12}}{\tau_1} \quad (14)$$

$$J_{21e} = \frac{M_{1e}\phi_{12}}{\tau_1} - \left(\frac{f}{1-f}\right) \frac{M_{1e}(1 - \phi_{12})}{\tau_1} \quad (15)$$

When the system departs from equilibrium due, for example, to a change of climate on a timescale that is shorter, say, than the residence time τ_2 , it may affect the fluxes through which the reservoirs are interconnected or the carbon isotopic change that occurs in photosynthesis. The above described elements of the carbon cycle could then evolve dynamically and the equations that describe them must be solved numerically. In order to solve the governing equations, we need to specify the parameter dependences of the quantities δ_i , J_i , J_{12} , J_{21} , b_1 , b_2 , and ε_0 . Among these quantities, δ_i , J_i are especially important, but on the extremely long timescales of interest here the flux of inorganic carbon into the atmosphere due to volcanic outgassing may be compensated either entirely or in significant part by the draw down of this CO_2 into the oceans due to the alkalinity that is continuously added to the oceans due to calcium-magnesium silicate weathering of the continents. For the purpose of the initial stage of the analyses to follow, as in the work of *Peltier et al.* [2007], we will assume that the CO_2 added to the atmosphere by volcanic outgassing is balanced by the burial flux b_1 so that the influence of volcanic outgassing is short circuited. Of course such precision of balance is unlikely to have obtained but the precise degree of imbalance that may have existed is impossible to describe in a deterministic fashion. To this end, we will assume that this unbalanced perturbation of the $p\text{CO}_2$ can be represented stochastically following the methodology employed by *Stastna and Peltier* [2007]. Specifically, we will assume that the flux J_{12} will remain stable, an assumption that neglects fertilization effects which we will discuss further below, whereas the flux J_{21} will be considered to depend critically upon surface climate. This is reasonable in circumstances in which the total carbon assay is dominated by the organic fraction.

[12] In the model we have constructed, the variations of J_{21} and ε_0 are assumed to be an indirect consequence of the temperature dependence of the solubility of oxygen in seawater since by Neoproterozoic time the concentration of oxygen in the atmosphere is assumed to have reached a level close to modern [*Catling and Zahnle*, 2003; *Fike et al.*, 2006; *Holland*, 2006], the importance of which is further discussed in section 3.6. On the basis of the measurements

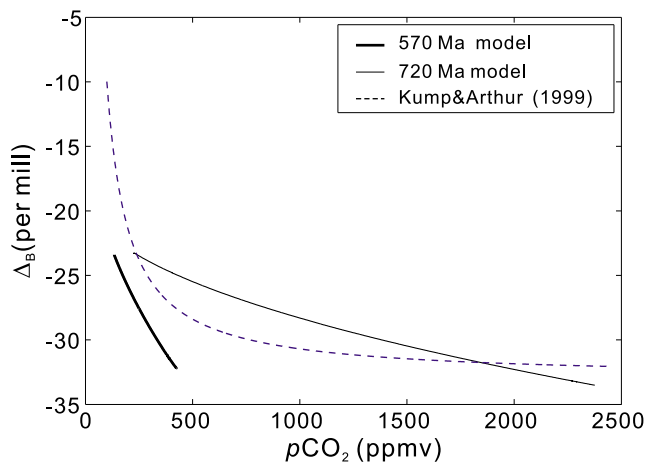


Figure 3. Comparison of the parameterization of the isotopic fractionation employed in the 570 Ma model (thick solid line) and 720 Ma model (thin solid line), respectively, to give the best fit to the observations with the parameterization (dashed line) obtained by *Kump and Arthur* [1999] for the Phanerozoic. Δ_B in both this figure and in Figure 2 of *Kump and Arthur* [1999] is essentially equivalent to $-\varepsilon_0$ in the text of this paper.

by *García and Gordon* [1992], one may justify a linear parameterization of the solubility of oxygen in seawater as:

$$O_{2,sol} = O_{2,sol_e} - A(T - T_e) \quad (16)$$

where T is taken to be the annually averaged global mean sea level temperature. The deviation of oxygen solubility away from its value at an equilibrium temperature, T_e , will tend to enhance or to weaken the remineralization flux J_{21} relative to its equilibrium value. Since no quantitative measurements are known to us regarding the relationship between the rate of remineralization of organic carbon and the oxygen concentration in seawater, we assume that this relationship is also linear as

$$J_{21} = J_{21_e} \left\{ 1 + B \left(\frac{O_{2,sol} - O_{2,sol_e}}{O_{2,sol_e}} \right) \right\}. \quad (17)$$

Substitution of equation (16) into (17) results in

$$J_{21} = J_{21_e} \{ 1 - F_{21}(T - T_e) \}. \quad (18)$$

where the critical control variable of the model is defined as:

$$F_{21} = \frac{AB}{O_{2,sol_e}}, \quad (19)$$

In equation (18), J_{21} is now directly dependent on the deviation of temperature through the newly defined parameter F_{21} , a parameter that has the dimensions of inverse temperature. In other words, this parameter determines the rate at which the atmospheric carbon cycle responds to climate change and is the most important parameter that determines the behavior of the coupled model. As shown in the work of *Peltier et al.* [2007], the magnitude of this parameter determines the period of the glacial cycles that, under certain

conditions, the model may support. In the low temperature vicinity of 1°C , $A \approx 8 \mu\text{mol}/(\text{kg } ^\circ\text{C})$ and $O_{2,sol} \approx 400 \mu\text{mol}/\text{kg}$ [*García and Gordon*, 1992]. The parameter B that contributes to determination of the strength of the dependence of the remineralization flux upon oxygen solubility will however also be dependent on ocean dynamics, temperature, and bulk chemical composition. This parameter is therefore completely unconstrained, which requires that a range of values for the parameter F_{21} be considered. For example, if the remineralization flux changes by 1.5% when oxygen solubility is doubled relative to its equilibrium value, then $F_{21} \approx 3 \times 10^{-4}$ per degree Centigrade. Since our purpose here is to investigate the robustness of the model in the presence of stochastic perturbations, a value of 1.5×10^{-4} per degree Centigrade for F_{21} will be employed in most of the investigations to be reported herein. The reason we choose this value is that the carbon cycle coupled climate system will exhibit relatively short period glacial cycles so that it will be unnecessary to run the model for very long times in order to simulate a representative sample of such events. Investigations which employ different values of F_{21} are also reported in order to demonstrate that the influence of stochastic perturbations is not significantly dependent on the value of F_{21} . This choice $F_{21} = 1.5 \times 10^{-4}$ per degree Centigrade leads to a predicted period of a typical glacial cycle of ~ 3 Myr in the analysis of *Peltier et al.* [2007]. Further discussion concerning the value of F_{21} is presented below in section 3.4.

[13] To adequately model the evolution of the isotopic composition of the carbon reservoirs, it is necessary to consider the influence of the concentration of dissolved CO_2 in seawater on the photosynthetic fractionation process of phytoplankton [*Kump and Arthur*, 1999]. As in the work of *Peltier et al.* [2007], the following parameterization is employed:

$$\varepsilon_0 = \varepsilon_{0_e} + \beta_{frac,M}(M_1(t) - M_{1_e}), \quad (20)$$

in which ε_{0_e} is the equilibrium value of the photosynthetic fractionation by Neoproterozoic organisms, $\beta_{frac,M}$ is specified so that model output $\delta^{13}\text{C}$ for the inorganic carbon reservoir ($\delta^{13}\text{C}_{inorg}$) best fits observed values. Note that in equation (20), the CO_2 concentration in the ocean is represented by the mass of total inorganic carbon. In the work of *Peltier et al.* [2007], ε_{0_e} was taken to be 28 per mil and the value of $\beta_{frac,M}$ that produced a best fit to the observations was found to be 0.00048 per mil per gigaton. Within the range of $p\text{CO}_2$ in our model, the value of ε_0 is not significantly different from that observed for the Phanerozoic Eon [*Kump and Arthur*, 1999] (ε_0 here is equivalent to $-\Delta_B$ in their paper), as shown by the thick line in Figure 3. The downward shift of ε_0 , or the relatively larger value of ε_0 for the Neoproterozoic than that for the Phanerozoic, is also consistent with that inferred by *Hayes et al.* [1999] and could be due to the difference in average growth rate, surface area-to-volume ratio of the cell, etc., between Phanerozoic and Neoproterozoic organisms.

[14] The set of nonlinear ordinary differential equations that replace the original equations (8)–(11) of *Rothman et al.* [2003] is obtained by substitution of a surface temperature modulated form of the equilibrium remineralization flux J_{21_e} and an appropriate parameterization for the dependence

upon climate of the photosynthetic isotopic fractionation ε_0 . Otherwise the fluxes that mediate the interactions between the reservoirs and the external environment are taken equal to their equilibrium values. The set of ordinary differential equations that this perturbation theory delivers is the following:

$$\begin{aligned} \dot{\delta}_1 = & \frac{J_{i_c}}{M_1} (\delta_i - \delta_1) + \frac{J_{21_c}}{M_1} (\delta_2 - \delta_1) (1 - F_{21} [T - T_e]) \\ & + \frac{J_{12_c}}{M_1} (\varepsilon_{0e} + \beta_{frac} [M_1 - M_{1e}]) \end{aligned} \quad (21)$$

$$\dot{\delta}_2 = \frac{J_{12_c}}{M_2} (\delta_1 - \delta_2 - [\varepsilon_{0e} + \beta_{frac} (M_1 - M_{1e})]) \quad (22)$$

$$\dot{M}_1 = -F_{21} J_{21_c} (T - T_e) \quad (23)$$

$$\dot{M}_2 = +F_{21} J_{21_c} (T - T_e) \quad (24)$$

where equations (23) and (24) are obtained by assuming $\phi_{12_c} \approx 1$ [Rothman *et al.*, 2003]. The model is then completely described by specifying values for the quantities ϕ_{12_c} , μ , τ_1 , ε_0 , δ_i , β_{frac} , T_e , and f . The values selected for these parameters for the calculations reported in this paper are essentially identical to those employed in the paper by Rothman *et al.* [2003] and are 0.999, 0.01, 1000 years, 28 per mil, -6 per mil, variable, 1°C, and 0.3, respectively. The value of ε_{0e} is changed to 25 per mil when the 720 Ma geography is employed in the model. This variation of ε_{0e} is consistent with the analysis of Hayes *et al.* [1999] for the Neoproterozoic (ε_0 here is essentially the same as ε_{TOC} in their paper), and is discussed in section 3.3. As in the work of Rothman *et al.* [2003], the selected values for ϕ_{12_c} and μ result in an organic reservoir mass that is approximately 100 times the mass of the inorganic reservoir. The initial mass of the inorganic carbon reservoir does not affect the dynamics in any way, but in our calculations has been initialized to the value of 40,000 Giga tons, as estimated by Kump and Arthur [1999] for the amount of inorganic carbon present in the modern ocean. The temperature employed for the purpose of coupling the carbon cycle to the model of the physical climate system is taken to be the annually averaged global mean sea level temperature.

[15] The modulation of the carbon cycle by the climate is effectively expressed by equations (16)–(19) above. In turn, the carbon cycle influences the climate by changing $p\text{CO}_2$ according to the following relationship between $p\text{CO}_2$ and M_1 ,

$$\frac{p\text{CO}_2(t)}{p\text{CO}_{2,e}} = \left[\frac{M_1(t)}{M_{1e}} \right]^X, \quad (25)$$

where the exponent X in the above power law relationship is suggested to be 2 by Kump and Arthur [1999] for the Phanerozoic, based on the assumption that the ocean was saturated with respect to calcite. A preliminary discussion of the validity of this assumption will be found in the work of Godd ris and Donnadieu [2008] and Peltier and Liu [2008], and a deeper discussion will be presented below in this

paper. Peltier *et al.* [2007] have also shown that model results are relatively insensitive to the specific choice of the value for X and thus are not critically dependent on the validity of that assumption.

[16] The incremental infrared radiative forcing at the surface due to the variation of CO_2 concentration relative to a reference level is formulated as follows:

$$d\text{Rad} = k \ln \left(\frac{p\text{CO}_2}{p\text{CO}_{2,e}} \right) \quad (26)$$

where $p\text{CO}_{2,e}$ is the reference level and has a value of 300 ppmv. Here k is a constant whose value may be obtained through radiative-convective modeling utilizing the known spectral absorption characteristics of CO_2 [Myhre and Stordal, 1997; Myhre *et al.*, 1998; Ramanathan *et al.*, 1979] for which a value of 6.0 W m^{-2} is assumed [Tarasov and Peltier, 1997, 1999].

[17] Therefore the climate system and the carbon cycle are physically coupled to each other through partitioning of O_2 and CO_2 between ocean and atmosphere, as depicted in Figure 2. In computing the evolution of the coupled carbon cycle climate system, the same time step is employed for the carbon cycle as for the ice sheet coupled climate model [Liu and Peltier, 2010], namely 500 years.

[18] It is clear from equations (23)–(24) that F_{21} controls the strength of the feedback that is critical to the model and is therefore an influence that must be thoroughly explored. However, the parameter T_e may also be important because it determines the direction of the feedback in a given climate state. For example, assuming that the mean surface temperature is 2°C, climate will warm if T_e is equal to 4°C, but will cool if T_e is equal to 0°C. Since T_e is also poorly constrained, we must also investigate the influence of this additional parameter.

2.2. Stochastic Component of Climate Forcing

[19] Variability in climate may arise due to the action of either external or internal mechanisms and may operate on a wide range of timescales. For example, variations in Earth's orbital configuration due to many body effects in the solar system cause changes in the latitudinal variation of the solar radiation at the top of the atmosphere (TOA) on timescales of 41,000 years and $\sim 20,000$ years (obliquity and precession), respectively. Other climatically important but shorter lived variations may be attributed to volcanic eruptions or meteorite impacts. The latter are of course examples of external sources of variability. The internally derived perturbations to the system that are of interest to us here are those associated with the carbon cycle though the impact of variations of the atmospheric concentrations of CO_2 and other greenhouse gases that are not explicitly modeled in the previously described theoretical structure. The processes affecting the unmodeled greenhouse gas (GHG) concentrations are primarily those associated with temporal variations of the volcanic outgassing source of atmospheric CO_2 and silicate weathering sink of atmospheric CO_2 , the balance between which throughout the Phanerozoic has prevented extreme variations in atmospheric $p\text{CO}_2$ [Berner, 2004]. Both of these processes may be taken to operate on timescales of millions of years. Other relevant processes might

be taken to include the melting of methane hydrates, the storage (or release) of CO₂ in (or from) the deep ocean, and the expansion and contraction of continental biomass, the timescales of which might vary from months to thousands of years. Many of these processes interact with the ocean and ice sheet dynamics and are not well understood even in the most recent literature. For example, the explanation of the variation of atmospheric GHG concentrations during the glacial cycles of the Late Quaternary remains illusive [Sigman *et al.*, 2010].

[20] Orbital forcing is included in all of the simulations to be presented below. Because neither the amplitude nor the phase of the orbital variations during Neoproterozoic time is known, we will simply employ the modern orbital configuration as a substitute. However, as will be demonstrated, the direct influence of this forcing is negligibly small. This may be due to the neglect of important feedback mechanisms in the model which are not well understood. For example, variations of continental ice volume during the past million years of Earth history correlate well with orbital insolation forcing [Shackleton *et al.*, 1990], but it is not understood how the weak influence of direct orbital forcing could cause the observed significant covariations of greenhouse gas concentrations and thereby influence the 100 kyr glacial cycles of the Late Quaternary. This forcing might also be considered to constitute a component of the stochastic forcing having long memory. In order to represent the variations of climate forcing due to this and all other possible sources, we will simply perturb the value of $d\text{rad}$ (which is the long-wave radiative forcing at Earth's surface due to variations of atmospheric $p\text{CO}_2$) in equation (26) stochastically. A normally distributed random number generator will be employed to generate the perturbations. The distribution so generated will be taken to have zero mean, and the standard deviation (σ) will be varied among different simulations in such a way as to enable us to determine the amplitude of the noise (as measured by 3σ) that the coupled model is able to tolerate, i.e., such that it may never enter the "hard snowball" state due to the action of the negative feedback present in the unperturbed version of the model. We will refer to this perturbation as $\Delta d\text{rad}$, an illustrative example of which is shown in Figure 4a.

[21] In each time step of the integration of the dynamical model (every 500 years), $d\text{rad}$ is determined first by the deterministic carbon cycle model, then this value is perturbed by a random number $\Delta d\text{rad}$, and thus the evolution of the surface climate is itself perturbed. In reality, stochastic perturbations may have significant memory, as recently discussed in connection with the forcing of a simple model of the thermohaline circulation in the work of Stastna and Peltier [2007]. Rather than being characterized by a white noise power spectrum the stochastic component of the forcing will then be characterized by a "red" spectrum with more power concentrated at lower frequency than at high. We may redden the stochastic component of the forcing simply by fixing $\Delta d\text{rad}$ for more than a single time step. In what follows we will demonstrate the impact of memory of the stochastic perturbation by comparing the results obtained in five sets of simulations, in which $\Delta d\text{rad}$ is fixed for 1, 20, 40, 80 time steps, respectively. The power spectra (Figure 4b) of these time series of $\Delta d\text{rad}$ demonstrate that the noise becomes progressively more highly concentrated

at lower frequency the longer the memory. Because the memory of the noise appears as a square waveform in the time series, it does not appear as a single peak in the frequency domain. Note that because both climate model and carbon cycle model respond immediately to such perturbations, the variability of $d\text{rad}$ may be significantly modified relative to that in a model in which no stochastic component of the forcing is active. Figure 4c shows an example of the oscillation of $d\text{rad}$ in a version of the carbon cycle coupled climate model in which no stochastic component of the forcing is active. It will be observed that the simulated history of model evolution is smooth, and $d\text{rad}$ varies on a time scale of millions of years with a fixed period. When stochastic forcing (memory = 20 time steps) is added to the model, the variation of $d\text{rad}$ now includes higher-frequency variability (Figure 4d). However, by comparing Figures 4c and 4d, it will be observed that the effect of the stochastic component may not be simply to add random fluctuations to the previously perfectly periodic variation of $d\text{rad}$. Rather, the solution in this particular case is fundamentally transformed. Although cyclic variability persists, the solution is no longer perfectly periodic. In the following sections of this paper our goal is to fully characterize the nature of the solutions that the coupled model delivers as a function of the properties of the stochastic component of the forcing.

2.3. Continental Configurations

[22] Three different continental configurations will be considered; the same 570 Ma geography which was employed in both Hyde *et al.* [2000] and Peltier *et al.* [2007], which is more appropriate for the Marinoan glaciation; a 720 Ma geography obtained by Li *et al.* [2008] for the Sturtian glaciation of the Neoproterozoic; and a shifted version of the Li *et al.* [2008] geography for 720 Ma produced by rotating his model continental configuration southward by 5° (we will refer to this as the shifted 720 Ma geography hereafter). The latter continental configuration is included because there are still large uncertainties in determining the paleocontinental latitude, and this uncertainty is at least 5° on average [Li *et al.*, 2008; Trindade and Macouin, 2007]. Although the uncertainties in both the paleolatitude and paleolongitude vary among different continental fragments, to simplify the discussion, we chose to shift the entire supercontinental configuration by 5° toward the south. Since the present paper is an extension of the work of Liu and Peltier [2010], the same solar constants employed in that paper are used here, i.e., the solar constant is reduced by 5.7% and 7.2% relative to the present value for the 570 Ma and 720 Ma continental configurations, respectively. These reductions following from the fact that the luminosity of a main sequence star such as our own Sun increases at the rate of ~1% per 100 million years as it ages [Gough, 1981].

2.4. Biogeochemical Assumptions Underlying the Model and Their Motivation

2.4.1. Oxidation of DOC

[23] In equations (17) and (18) above, it is implied that when O₂ is input into the Neoproterozoic ocean, the net effect is that the DOC is oxidized and DIC is increased. The validity of this assumption may not be entirely obvious since there remains much to learn concerning ocean biogeochemistry

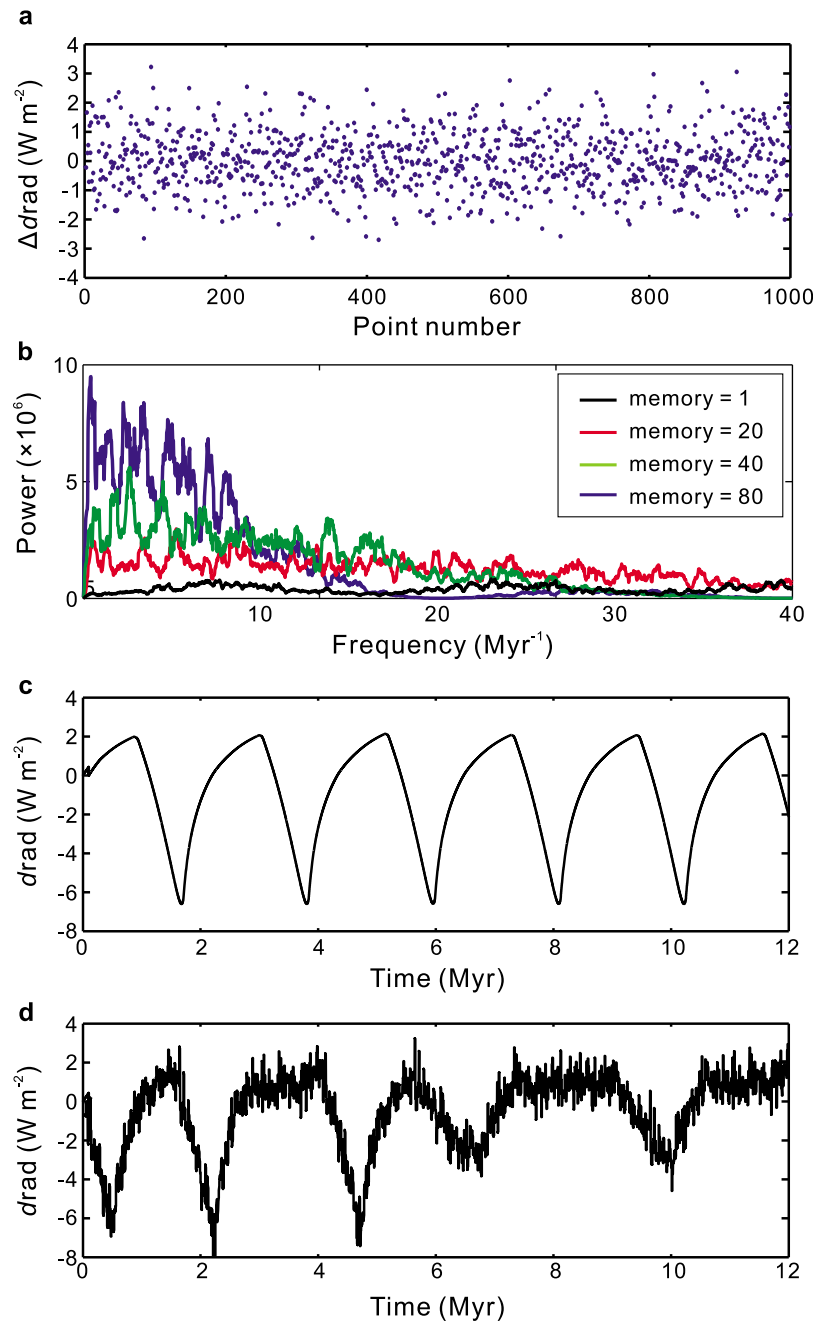


Figure 4. (a) A series of normally distributed random number, drad . (b) The Fourier analyses of the time series of noises. The noise series in Figure 4a is applied in the model with different memory, the values of which (in unit of time steps, with each time step equals to 500 years) are indicated in the legend. To show the red shift of the spectra as the memory of the noise is increased clearly, only the left most 1% of the whole spectra are shown. Note that the power of the spectrum for memory = 1 (gray curve) is already amplified by a factor of 6. (c) Variation of drad in a typical run of the carbon cycle coupled climate model with no noise perturbation considered. In this particular run, 570 Ma geography is employed and F_{21} is set to $0.0003^\circ\text{C}^{-1}$. (d) Variation of drad in the same run as Figure 4c, but here the noise perturbation of the form in Figure 4a is considered in the model.

even for the modern ocean. However, in the present context our goal is simply to establish the long timescale globally averaged variation of the system. We therefore ignore, for example, the detailed spatial distribution of nutrients by representing both the DIC and DOC reservoirs as well mixed, and all short timescale ($<$ timestep of the model,

i.e., 500 years) variations of the concentrations in these reservoirs. These additional sources of variability we assume to be captured by the stochastic component of the forcing. We expect that the globally averaged long timescale response of the biomass in the ocean to the input of oxygen

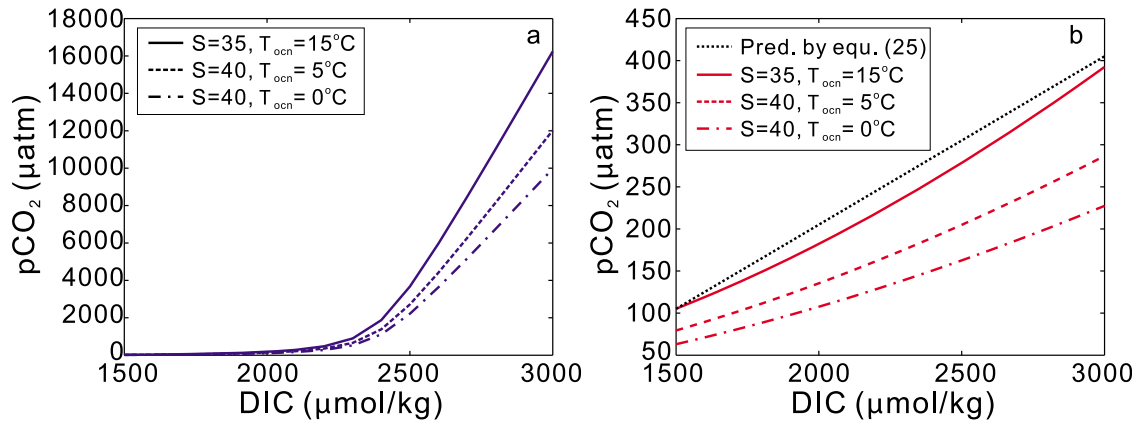


Figure 5. Relationship between $p\text{CO}_2$ and DIC when (a) alkalinity is fixed at $2400 \mu\text{mol/kg}$ and (b) alkalinity is increasing at same time linearly from 1900 to $3400 \mu\text{mol/kg}$. Different lines are for different settings of salinity (S) and temperature of the mixing layer ocean (T_{ocn}) as indicated by the legends. The dotted line in Figure 5b represents the prediction of the variation of $p\text{CO}_2$ with DIC by equation (25).

will be well predicted by equation (18) based upon the following considerations of the Neoproterozoic ocean.

[24] 1. Despite the fact that the atmosphere was oxygenated, the Neoproterozoic ocean (at least the deep ocean) remained anoxic until after the Marinoan glaciation [Canfield *et al.*, 2007, 2008; Fike *et al.*, 2006; Holland, 2006; McFadden *et al.*, 2008; Scott *et al.*, 2008]. Especially in the work of Canfield *et al.* [2008], it is argued that the ocean was largely anoxic below the mixed layer for much of the late Neoproterozoic.

[25] 2. The DOC in the ocean was thousands of times in excess of that in the modern ocean according to the Rothman *et al.* [2003] analysis, as supported by that of Fike *et al.* [2006]. Added to this is the fact that the ratio of DOC: phytoplankton is 200:1 in the modern ocean [Nagata, 2008]. If enough oxygen is supplied, bacterial respiration, the major DOC oxidation process [Ducklow, 2003] will be enhanced by orders of magnitude [Robinson, 2008] with such a high concentration of DOC in the seawater.

[26] 3. Bacterial respiration and photosynthetic fixation compete for nutrients [Church, 2008]. Especially, many bacteria have advantages over phytoplanktons in uptaking phosphorus [Joint *et al.*, 2002]. Therefore it is impossible that the nutrients and inorganic carbon released during bacterial respiration will be significantly utilized by primary producers.

[27] 4. Principal primary production is generated within the surface ocean (the euphotic zone), whereas bacterial respiration is most probably active in the whole ocean. Therefore we may safely assert that the oxidation of the massive DOC reservoir was oxygen limited. Any oxygen input into the ocean would enhance the oxidation process much more efficiently than the photosynthetic process, leading to an increase of DIC. An important fraction of this DIC will be partitioned into the atmosphere (see below), producing a negative feedback on hard snowball formation. Primary production might also benefit from the nutrients released during the remineralization of DOC, but this process must be slaved to the process of the oxygen driven remineralization. This is contrary to the modern ocean, in

which the bacterial respiration and production is often limited by primary production.

2.4.2. The $p\text{CO}_2$, DIC, and Alkalinity

[28] In calculating the atmospheric CO_2 concentration from the mass of DIC, we have adopted equation (25), which was obtained by Kump and Arthur [1999] for the Phanerozoic Eon. We have therefore elected to employ the same assumption as in Kump and Arthur [1999] that the ocean remained saturated with respect to calcium carbonate in the Neoproterozoic. The implications of this assumption and the requirements for it to remain valid are discussed in what follows.

[29] First we need to quantitatively calculate how CO_2 is partitioned between atmosphere and ocean when these two components of the system are in equilibrium, given DIC and alkalinity (ALK) concentration in the ocean without assuming that the ocean is saturated with respect to carbonate. The atmospheric $p\text{CO}_2$ can be calculated [Zeebe and Wolf-Gladrow, 2001] as follows. According to Henry's law,

$$p\text{CO}_2 = [\text{CO}_2]/K_h \quad (27)$$

where $[\text{CO}_2]$ is the sum of the concentration of aqueous CO_2 and H_2CO_3 in the seawater, and K_h is the temperature and salinity dependent solubility coefficient of CO_2 in seawater. $[\text{CO}_2]$ in equation (27) may be computed by solving the following two simultaneous equations involving both DIC and ALK as:

$$\text{DIC} = [\text{CO}_2] \left(1 + \frac{K_1^*}{[\text{H}^+]} + \frac{K_1^* \cdot K_2^*}{[\text{H}^+]^2} \right) \quad (28)$$

and

$$\text{Alk} = [\text{CO}_2] \left(\frac{K_1^*}{[\text{H}^+]} + 2 \frac{K_1^* \cdot K_2^*}{[\text{H}^+]^2} \right) + \frac{B_T K_B^*}{K_B^* + [\text{H}^+]} + \frac{K_W^*}{[\text{H}^+]} - [\text{H}^+] \quad (29)$$

where K_1^* and K_2^* are the first and second dissociation constants of carbonic acid, K_W^* and K_B^* are the dissociation

Table 1. Output of the Software in the Work of *Zeebe and Wolf-Gladrow* [2001] Given DIC and Alkalinity^a

DIC ($\mu\text{mol/kg}$)	ALK ($\mu\text{mol/kg}$)	$[\text{CO}_2]$ ($\mu\text{mol/kg}$)	$[\text{HCO}_3^-]$ ($\mu\text{mol/kg}$)	$[\text{CO}_3^{2-}]$ ($\mu\text{mol/kg}$)	$p\text{CO}_2$ (μatm)	pH Total
1500	2400	0.83157	887.056	612.112	22.1996	8.96759
1600	2400	1.31158	1052.41	546.274	35.0136	8.84393
1700	2400	2.00268	1218.45	479.550	53.4630	8.72374
1800	2400	3.00672	1384.55	412.439	80.2665	8.60276
1900	2400	4.50185	1550.19	345.311	120.180	8.47653
2000	2400	6.82749	1714.62	278.552	182.265	8.33945
2100	2400	10.7068	1876.54	212.757	285.827	8.18324
2200	2400	17.9170	2032.88	149.207	478.306	7.99439
2300	2400	33.4896	2175.12	91.3882	894.027	7.75211
2400	2400	70.1369	2281.84	48.0237	1872.35	7.45188
2500	2400	137.482	2336.82	25.6944	3670.17	7.16992
2600	2400	223.463	2360.41	16.1288	5965.49	6.96332
2700	2400	316.644	2371.86	11.4932	8453.03	6.81406
2800	2400	412.757	2378.38	8.86541	11018.8	6.70013
2900	2400	510.271	2382.53	7.19629	13622.0	6.60878
3000	2400	608.547	2385.40	6.04870	16245.6	6.53281

^aTemperature and salinity of the ocean are assumed to be 15°C and 35 per mil, respectively. In this calculation, alkalinity is fixed at 2400 $\mu\text{mol/kg}$, while DIC is varied (the shaded column). In the variables below, $[\text{CO}_2]$ represents the concentration of aqueous CO_2 plus H_2CO_3 , ALK represents alkalinity, pH Total represents the pH value in total scale.

constants of water and boric acid, respectively, all of which are mainly temperature and salinity dependent and empirically determined [*Zeebe and Wolf-Gladrow*, 2001]. B_T is the total boron concentration given by $416 \cdot (S/35) \mu\text{mol/kg}$ [*Zeebe and Wolf-Gladrow*, 2001], where S is salinity of the seawater. From equations (28) and (29), the concentration of protons, $[\text{H}^+]$, in the seawater and thus pH is obtained simultaneously with $[\text{CO}_2]$. Moreover, $[\text{HCO}_3^-]$ and $[\text{CO}_3^{2-}]$ can be easily calculated through the definitions of K_1^* and K_2^* , respectively.

[30] We have solved the above equations by employing the software provided by *Zeebe and Wolf-Gladrow* [2001]. As basis for the analyses required, the following properties of the Neoproterozoic ocean were initially assumed, namely that the average salinity of the ocean was 35 per mil and the temperature of the mixed layer of the ocean was 15°C, respectively, and that the typical values for DIC and alkalinity of the seawater were close to modern, i.e., 2000 $\mu\text{mol/kg}$ and 2400 $\mu\text{mol/kg}$, respectively. If we further assume that the atmospheric pressure is 1 bar, then the variation of $p\text{CO}_2$ in the atmosphere corresponding to a change of DIC from 1500 to 3000 $\mu\text{mol/kg}$ while the alkalinity is fixed at 2400 $\mu\text{mol/kg}$ can be calculated. The result of the calculation is displayed in Figure 5a (solid line), which shows that $p\text{CO}_2$ rises dramatically from ~180 ppmv when DIC is 2000 $\mu\text{mol/kg}$ to over 15000 ppmv when DIC is 3000 $\mu\text{mol/kg}$, much faster than the quadratic rate embodied in equation (25). A listing of the data delivered by the *Zeebe and Wolf-Gladrow* [2001] procedure are shown in Table 1. During this increase of $p\text{CO}_2$, the ocean becomes undersaturated with respect to calcium carbonate so that the condition for equation (25) to be valid is violated. However, the calculation demonstrates the important fact that equation (25) provides only a lower bound for how much CO_2 can be partitioned into the atmosphere through remineralization of DOC in the ocean. Therefore the negative feedback introduced by *Peltier et al.* [2007] to prevent the occurrence of a “hard snowball” becomes significantly stronger if equation (25) is rendered invalid by the onset of calcium carbonate undersaturation.

[31] Apparently, an increased input of alkalinity is required in order for the quadratic relationship between $p\text{CO}_2$ and DIC in equation (25) to remain valid as $p\text{CO}_2$ in the atmosphere rises. To demonstrate this, we assume that the alkalinity would increase linearly with DIC, and on this basis the result obtained is shown in Figure 5b (solid line), which is very close to the prediction of equation (25) (dotted line in Figure 5b). The detailed data derived from the *Zeebe and Wolf-Gladrow* [2001] calculation concerning the alkalinity increase is presented in Table S1 of the auxiliary material.¹ This fully verifies the point in the work of *Godd eris and Donnadi eu* [2008] that alkalinity needs to be increased during the warming phase of the glacial cycle in order for the relationship embodied in equation (25) to remain valid. However, these authors failed to point out that the strength of the negative feedback actually benefits from the failure of equation (25) rather than being undermined by such failure. The paradox claimed to be characteristic of our model by *Godd eris and Donnadi eu* [2008] is therefore nonexistent. Moreover, since most of the continents are covered by land ice during the glacial phase of the cycle (Figure 6 here and Figure 5 in the work of *Peltier et al.* [2007]), the alkalinity input from the continents into the oceans due to silicate weathering could be diminished rather than increased. The actual CO_2 production in the atmosphere due to the increase of DIC in the ocean could be much higher than that obtained from equation (25). However, it is very possible that the alkalinity in the ocean will continue to grow because the sink for carbonate alkalinity (i.e., the precipitation of carbonate ions out of the ocean to form carbonate rocks on the sea floor) is even more severely reduced and the source of alkalinity is continuously generated primarily from carbonate weathering of the continents, as described in detail below.

[32] It is evident that in solving equations (27)–(29), an assumption must be made concerning ocean temperature (the temperature of the mixed layer is probably most

¹Auxiliary materials are available in the HTML. doi:10.1029/2010JD015128.

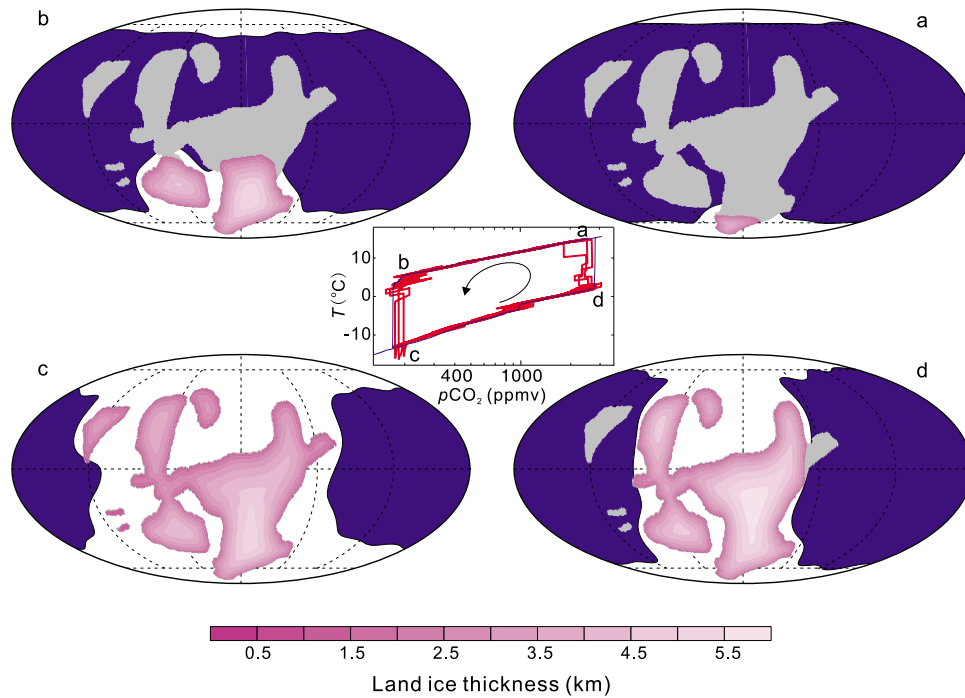


Figure 6. Snapshots of ice distribution for simulation at the four corners of the hysteresis loop for the 720 Ma continental configuration in temperature $-p\text{CO}_2$ solution space. The blue curve is the hysteresis loop consisting of the steady states of the climate model without coupling with the carbon cycle model. The hysteresis loop (blue line) is the same as the red line in Figure 1. The red curve shows the evolution of the coupled model under the perturbation of stochastic noises, and the direction of the evolution is indicated by the curved arrow. It is from the same simulation as that in Figure 12j. Pink and white represent land ice and sea ice, respectively, and blue represents the ocean.

appropriate). This differs from the mean surface temperature that is employed in solving the equations that govern the carbon cycle in section 2.1. Although the mean surface temperature can be very low during a typical glacial cycle (Figures 6 and 7), the ocean mixed layer temperature cannot

be much lower than 0°C but could be well below the value of 15°C that is employed in the example above. Moreover, the salinity of the ocean would undoubtedly be much higher than modern due to removal of the freshwater from the oceans required to build the massive accumulations of land

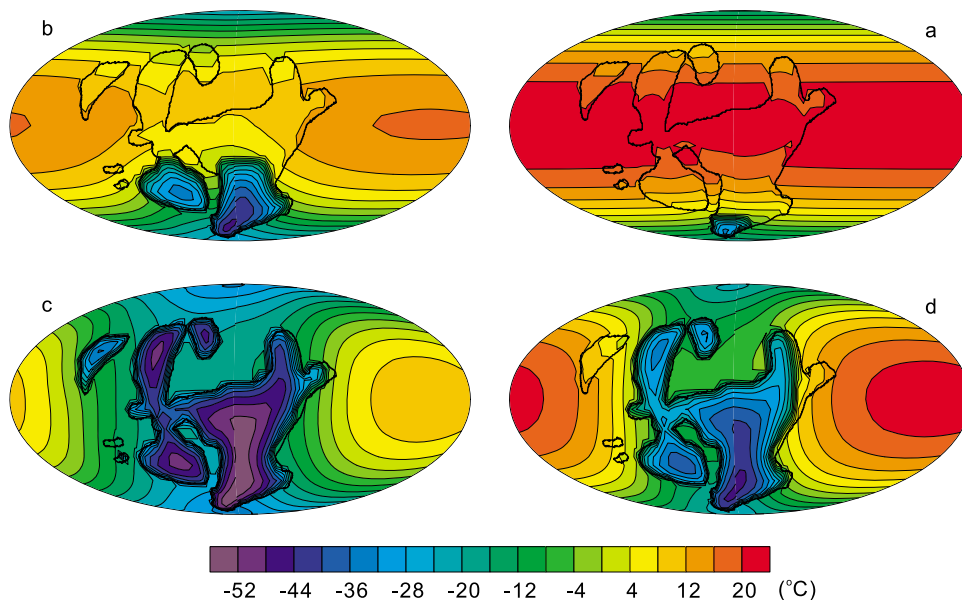


Figure 7. Temperature distribution corresponding to the ice distribution shown in Figure 6.

ice (Figure 6). We have therefore repeated the above described calculations under the assumptions that temperature and salinity were changed to 5°C and 40 per mil and 0°C and 40 per mil, respectively. The results are also shown in Figure 5, and the data are presented in Tables S2–S5 of the auxiliary material. It is clear on the basis of the results of these analyses that less CO₂ will be partitioned into the atmosphere for the same DIC and alkalinity due to the lower ocean temperature (the effect of the higher salinity is actually opposite but small; results are not shown), but the *p*CO₂ still increases rapidly with increasing DIC, especially when the ocean is not saturated with respect to calcium carbonate (Figure 5a). These results contradict the claim in the work of Hoffman *et al.* [2008] that the increased solubility of CO₂ in the ocean as temperature decreases would counter the effect of the negative feedback introduced by Peltier *et al.* [2007]. The decrease of *p*CO₂ due to its increased solubility does not persist and is quickly dominated by the increase of *p*CO₂ due to the increase of the mass of DIC through remineralization of DOC. It is uncertain which of these two processes dominates during the transition of the climate from a relatively warm state to a “soft snowball” state. However, because the equilibration time of CO₂ with seawater is 20 times longer than that of O₂ with seawater [Zeebe and Wolf-Gladrow, 2001], it is possible that the effect of the increased solubility of CO₂ in seawater may be negligible even at the beginning of the cooling phase of the cycles if the remineralization of DOC is rapid. As pointed out by Peltier and Liu [2008], the ocean carbon cycle is a buffered system with respect to CO₂ uptake. There is no similar resistance to the uptake of oxygen.

[33] Clearly, assuming that the ocean remained saturated with respect to carbonate during the Neoproterozoic glacial cycles makes the negative feedback associated with DOC remineralization the weakest possible which therefore makes the system most susceptible to descent into a “hard snowball” state under stochastic perturbation. All of the calculations presented in this paper are therefore based upon this assumption because it is entirely possible that the Neoproterozoic ocean remained saturated with respect to carbonate even during the glacial phase of the oscillatory cycle. This can be understood by inspecting the primary source and sink of ocean (carbonate) alkalinity. These are both expected to adjust to the onset of continental glaciation. It may be expected, however, for the sink to have reacted most strongly by diminishing in strength for two reasons [Ridgwell *et al.*, 2003]: namely, (1) the total neritic area available for carbonate deposition may have been greatly reduced and (2) calcareous plankton that dominate carbonate deposition in the modern open ocean were probably absent or rare. In fact, Ridgwell *et al.* [2003] argue that the Neoproterozoic ocean might have been supersaturated with respect to carbonate for these reasons.

[34] The major source of alkalinity should still have been derivative of continental weathering. While there has been relatively little research done on chemical weathering beneath polar ice sheets due to the difficulty of access (S. Anderson, personal communication, 2010), abundant research has been done on subglacial weathering beneath temperate glaciers (see review of Anderson [2007]). The chemical weathering expected in a soft snowball state may be approached from the perspective of these temperate

studies [Tranter *et al.*, 2002] since most of the soft snowball ice sheets are found in tropical to temperate regions. This research has generally shown that chemical weathering is continuous under wet based glaciers and that the cation output remains high, mainly due to the dissolution of carbonates regardless of bedrock type [Anderson, 2007]. This dissolution of carbonate is enhanced by the finer grains generated through grinding at the ice sheet base. Furthermore, the discharge from such ice sheets into the ocean also carries unweathered materials into the ocean which can be weathered quickly in the seawater [Gislason *et al.*, 2006; Stefánsdóttir and Gislason, 2005]. Another significant factor which must be considered is that large amounts of carbonate will be exposed to both physical and chemical weathering during a soft snowball state due to the fall of sea level caused by land ice development. The increased weathering rate of exposed carbonate has been shown to have been significant during the Last Glacial Maximum [Gibbs and Kump, 1994]. It should also be noted that the net uptake of atmospheric CO₂ in generating alkalinity described above is small since the portion of alkalinity delivered through silicate weathering is very small. Other sources of alkalinity may also be found, e.g., bacterial sulfate reduction, as mentioned previously by Peltier and Liu [2008].

[35] Assuming that carbonate precipitation is negligible and that the long-term alkalinity input into the ocean is balanced by volcanic outgassing as in the work of Munhoven and Francois [1994], the annual input of alkalinity into the ocean is 14×10^{12} eq. Further assuming that the ocean volume is similar to modern (Neoproterozoic ocean area was probably larger, but the depth is smaller in a soft snowball), i.e., 1.35×10^{18} m³, the alkalinity of the ocean will increase at a rate of approximately $10 \mu\text{mol kg}^{-1} \text{ kyr}^{-1}$ or $10^4 \mu\text{mol kg}^{-1} \text{ Myr}^{-1}$, much larger than the rate assumed in the calculation in our paper ($500 \mu\text{mol kg}^{-1} \text{ Myr}^{-1}$ if the duration of the soft snowball is 3 Myr). Therefore only when the rate of alkalinity input is reduced by a factor of 20 compared to the long-term average rate will the ocean become undersaturated.

[36] We must therefore consider, in our investigation of the resilience of the system against hard snowball formation, the limiting case that the ocean remained saturated with respect to carbonate. If ice sheet derived weathering were insufficiently effective, the activity of the carbonate system would entirely prevent descent into any snowball state, hard or soft, due to lack of alkalinity.

3. Results and Discussion

3.1. Limit Cycle Behavior in the Absence of Stochastic Perturbations

[37] Figures 8–10 show the time series of mean sea level temperature from runs employing the previously described three continental configurations. Only the results for runs of the model in which the control parameter F_{21} equals 0.0003 or $0.00015^\circ\text{C}^{-1}$ are shown here due to the limitations of space; additional results for F_{21} values of 0.001 and $0.0005^\circ\text{C}^{-1}$ are made available as auxiliary material (see Figures S1–S3 there). For each F_{21} value, the reference temperature is varied from 0 to 4°C and from 1 to 4°C for the 570 Ma and 720 continental configurations, respectively, to investigate

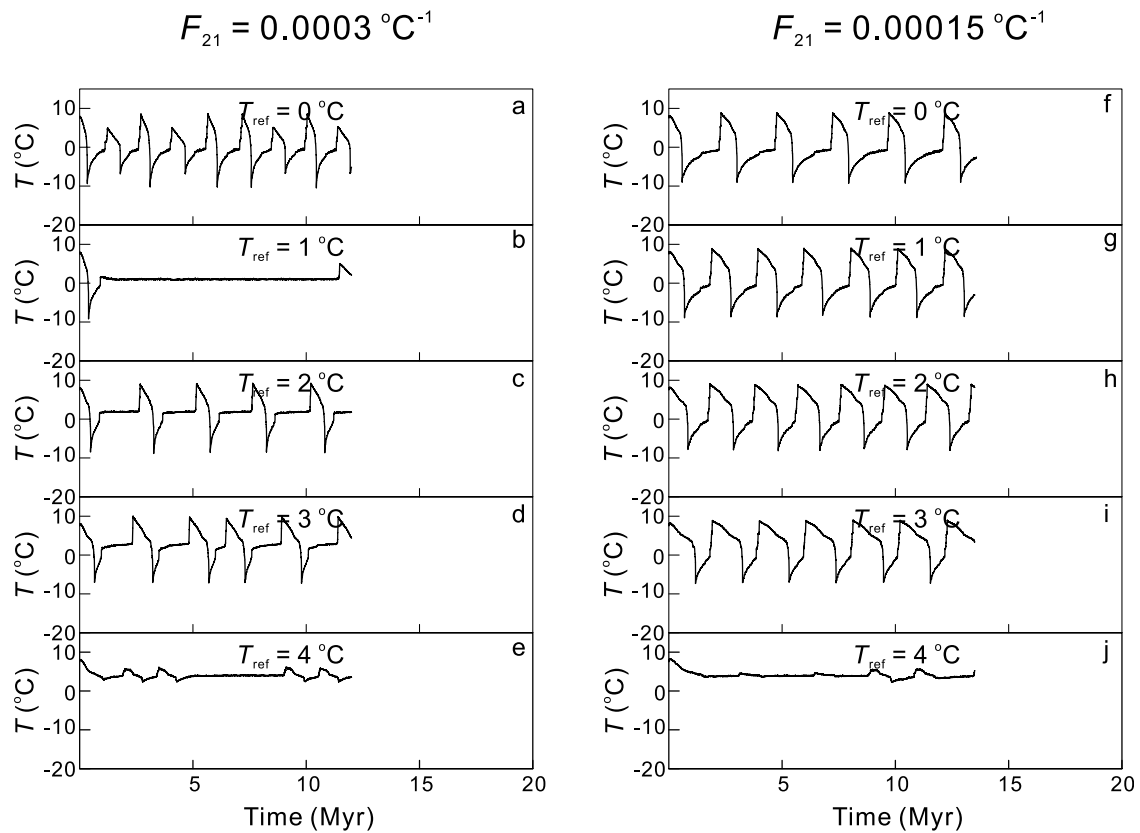


Figure 8. Time series of mean sea level temperature for runs in which the 570 Ma continental configuration is employed, and no stochastic perturbation is applied. The control parameter F_{21} is equal to 0.0003 and $0.00015^{\circ}\text{C}^{-1}$ for the left and right column, respectively. The reference temperature for each run is indicated by T_{ref} .

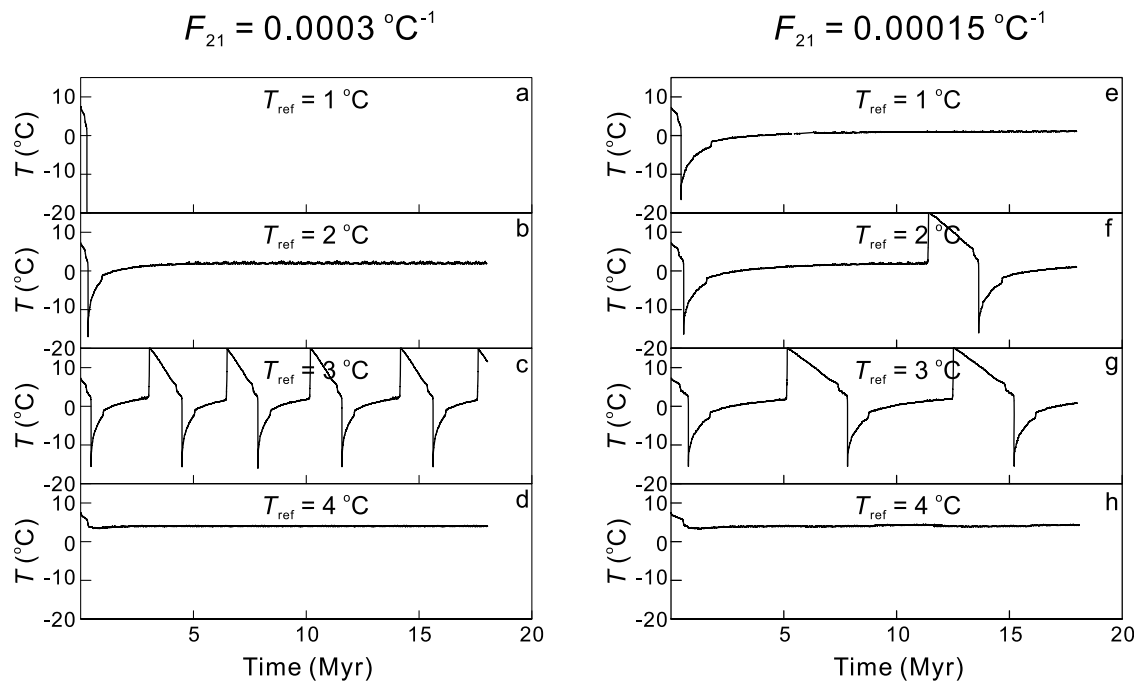


Figure 9. Similar to those in Figure 8 except that these are for the 720 Ma continental configuration as reconstructed by *Li et al.* [2008] with connectivity between continental fragments increased (see *Liu and Peltier* [2010]).

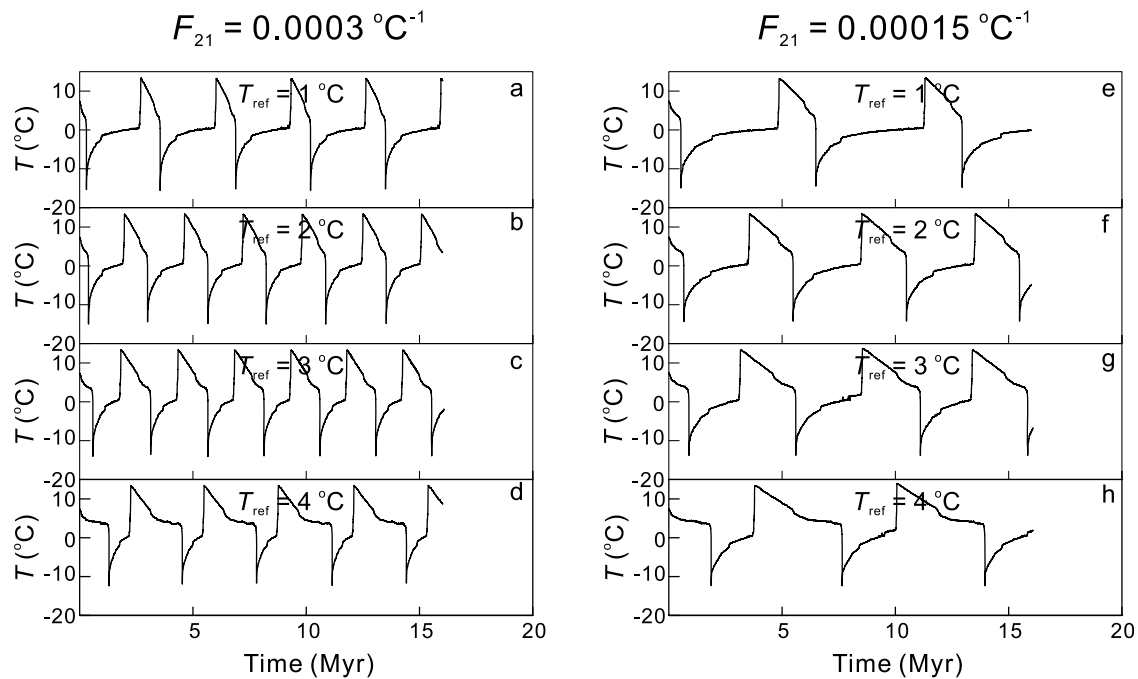


Figure 10. Similar to those in Figure 9 except that these are for the shifted 720 Ma continental configuration.

the influence of the reference temperature on the dynamics of the system. It will be clear by inspection of these results that the reference temperature is a further control variable of the model. In the range of reference temperatures tested, the dynamics of the system for both the 570 Ma and 720 Ma continental configurations switch between limit cycle and steady state (or fixed point in the temperature- $p\text{CO}_2$ space, not shown) at a fixed value of F_{21} (see, for example, Figures 8 and 9 and Figures S1–S2 of the auxiliary material).

[38] For the 570 Ma geography, the system exhibits cyclic behavior for most of the reference temperature and F_{21} values tested. This is consistent with the results reported by *Peltier et al.* [2007] that when the reference temperature is 0°C , the period of the oscillations decreases monotonically with the increase of F_{21} (Figure 8 here and Figure S1 of the auxiliary material). However, this simple relationship is violated at other reference temperatures. For example, at a reference temperature of 2°C , the period increases when F_{21} is increased by a factor of 2 from $0.00015^\circ\text{C}^{-1}$ to $0.0003^\circ\text{C}^{-1}$ (Figures 8c and 8h) but decreases again when F_{21} is increased from $0.0005^\circ\text{C}^{-1}$ to 0.001°C^{-1} (Figures S1c and S1h of the auxiliary material). This complication is partially attributed to the influence of orbital perturbations, without which the system will enter a steady state with mean sea level temperature equal to the reference temperature (result not shown but can be inferred from Figure 8c, in which the mean sea level temperature tends to remain constant). The relationship between the period of oscillation and the reference temperature is most clearly seen from Figures 8f–8j, where the value of F_{21} is fixed to $0.00015^\circ\text{C}^{-1}$. The period first decreases with increasing reference temperature and then increases again. This is reasonable since when the reference temperature is high, the climate warms faster from the “soft snowball” state due to stronger negative feedback (the absolute value of the right-hand side of equation (23) is

larger), so that the cold phase of the oscillations is reduced in duration and the period shortens. When the reference temperature is very high, however, it takes longer for the climate to cool from a warm state toward a “soft snowball” state; hence the warm phase of the oscillation expands and the period increases once more. Especially when the reference temperature is as high as 4°C (Figures 8e and 8j), the system never descends into the cold state but rather evolves into a steady state at the reference temperature.

[39] When the reference temperature is low, the model may predict only a single glacial event following which the system returns to a steady state at the reference temperature (e.g., Figures S1a and S1b of the auxiliary material). This is because, as climate evolves from a “soft snowball” state toward the warm state under the action of the negative feedback but before it can return to the warm state, the temperature of the system rises to a value close to the reference temperature, and the negative feedback becomes extremely weak, essentially vanishing.

[40] The influence of orbital forcing is also evident in the almost time-independent portion of the time series in Figure 8b, in which small amplitude quasiperiodic oscillations are superimposed upon the glaciation signal. Detailed comparison of the results in Figure 8 with those presented by *Peltier et al.* [2007], not shown, reveal the influence of the small amplitude orbital perturbation very clearly.

[41] In the case of the 720 Ma geography, oscillatory solutions exist only for the reference temperatures of 2 and 3°C , whereas isolated single glaciation event solutions are more likely for lower reference temperatures (Figure 9). For this configuration of the supercontinent, the model climate is more likely to enter the “hard snowball” state (Figure 9 and Figure S2 of the auxiliary material) compared to that for the 570 Ma geography when reference temperature is low. The

reason for this is that the 720 Ma model is more sensitive to the rate at which atmospheric $p\text{CO}_2$ decreases, as explained by *Liu and Peltier* [2010]. The rate of variation of the atmospheric $p\text{CO}_2$ is determined by the coupling between the carbon cycle and climate, more specifically by the absolute value of the right-hand side of equation (23). Therefore the lower the reference temperature, the faster the $p\text{CO}_2$ will decrease if the initial climate is warm. However, the sensitivity to the rate of variation of $p\text{CO}_2$ is much reduced if the configuration of the supercontinent is shifted toward the South Pole by 5° , the major effect of which is that land ice is now able to develop at relatively high $p\text{CO}_2$ levels as explained in detail in the work of *Liu and Peltier* [2010]. With this slight shift in the latitudinal centroid of the supercontinent the system never enters the “hard snowball” state for the majority of model runs (Figure 10 and Figure S3 of the auxiliary material).

[42] The reference temperature assumed in the model is clearly unconstrained observationally. However, it is reasonable to assume that the reference temperature for the 720 Ma continental configuration was higher than that for the 570 Ma configuration. Earth’s climate had been warm from ~ 2 billion years ago to ~ 800 Ma and then appears to have cooled gradually into the Cryogenian Period. This cooling may have been due to enhanced silicate weathering associated with the breakup of the supercontinent of Rodinia [*Donnadieu et al.*, 2004]. If this cooling trend continued from 720 Ma to 570 Ma, then it is most probably appropriate to choose a higher reference temperature for the Sturtian glaciation than that for the Marinoan glaciation. For consistency with *Peltier et al.* [2007], 0°C is again chosen to be the reference temperature for the 570 Ma model, and only the results for the reference temperature of 4°C for both the original and shifted 720 Ma geographies will be presented in what follows. Results for other reference temperatures are provided in the SOM.

3.2. Influence of Stochastic Perturbations

[43] For the 570 Ma geography, results are presented only for runs in which $F_{21} = 0.00015^\circ\text{C}^{-1}$ and reference temperature is equal to 0°C (Figure 11). Results for additional values of F_{21} of 0.0003, 0.0005, and 0.001°C^{-1} are presented in the SOM (Figures S4–S6 of the auxiliary material). For each value of F_{21} , 16 cases were explicitly analyzed and are organized into four sequences in Figure 11 (and Figures S4–S6 of the auxiliary material) according to the memory assumed for the stochastic noise. In each sequence, the amplitude of the noise increases from 1 W m^{-2} to 4 W m^{-2} , where 1 W m^{-2} is approximately equivalent to an 18% change of $p\text{CO}_2$ and 4 W m^{-2} is equivalent to doubling or halving $p\text{CO}_2$. As shown in Figure 11, climate for the 570 Ma geography is stable when subject to perturbations with amplitude up to 4 W m^{-2} . By stable, we mean that the climate system never descends into a “hard snowball” state even when subjected to stochastic perturbations. However, when the value of F_{21} is increased by a factor of 2 from 0.00015 to $0.0003^\circ\text{C}^{-1}$ (Figure S4 in auxiliary material), the climate system does descend into this state when the amplitude of the stochastic perturbations reaches 3 W m^{-2} , and becomes more susceptible to such perturbations with further increase of the F_{21} value (Figures S5 and S6 of the auxiliary material). Decreasing the value of F_{21} from

$0.00015^\circ\text{C}^{-1}$, of course, will lead to increased stabilization of the system (results not shown).

[44] The climate system also displays nonmonotonic variability to perturbations with the same amplitude but with different memory (Figure S4 of the SOM). This is entirely reasonable since an ice sheet takes thousands of years to respond significantly to any perturbation in the forcing. The longer an applied fluctuation in the forcing is maintained the more significant the impact upon climate state. On the other hand, if the memory of the fluctuations is excessive, perturbations during the course of a 20 Myr simulation will be infrequent and therefore a fluctuation of the appropriate sign to trigger snowball onset will be improbable. This is most clearly demonstrated by comparing the runs with noise of 3 W m^{-2} but with different memories in Figure S4 of the auxiliary material, where the system descends into a “hard snowball” state for memories of 20 and 40 time steps but survived the perturbations for memory of 80 time steps. It is reasonable to assume that fluctuations present in the natural system contain components of all frequencies and we may therefore take the largest amplitude perturbation for which the system is able to resist descent into the “hard snowball” state for all values of the memory to define a critical stochastic amplitude.

[45] It is also evident in Figure 11 that the period of the oscillations decreases as the amplitude of the stochastic perturbations is increased. This is unsurprising since cyclic glaciation is associated with the cyclic evolution of the climate system between the warm branch and oasis branch of the hysteresis loop (*Liu and Peltier* [2010] and Figure 1 here). In the absence of stochastic perturbations, the climate evolves gradually toward a critical point at which it then rapidly jumps from the warm branch to the cold branch or vice versa. In the presence of stochastic perturbations, however, this critical point may be reached much earlier, therefore leading to a reduction of the period of the glacial cycles.

[46] In comparison to this solution for glacial climate in the model with 570 Ma geography, the climate in the model with 720 Ma geography is more unstable. For runs (Figure 12) with F_{21} equal to $0.00015^\circ\text{C}^{-1}$ and reference temperature equal to 4°C , the critical amplitude of the perturbation is reduced to 3 W m^{-2} . This critical amplitude of the perturbation is further reduced to 2 W m^{-2} if the reference temperature is lower than 4°C (Figures S7–S9 of the auxiliary material). Comparison of Figure 12 with Figure 9h shows that steady solutions become oscillatory solutions due to the action of stochastic perturbations. This further demonstrates the significance of introducing noise into the system. As expected, when the value of F_{21} is increased to $0.0005^\circ\text{C}^{-1}$, the period of the glacial oscillations increases but the critical amplitude of the perturbation stays the same (Figure S10 of the auxiliary material).

[47] If the 720 Ma continental configuration is shifted by 5° toward the South Pole, however, climate is strongly stabilized. Figure 13 shows that the climate for the shifted 720 Ma geography is stable under perturbations with amplitude of 4 W m^{-2} , using the same F_{21} and reference temperature as those employed to construct the solutions shown in Figure 12. Results for other reference temperatures are presented in the auxiliary material (Figures S11–S13 of the auxiliary material), which demonstrates again that the

$$T_{\text{ref}} = 0 \text{ } ^\circ\text{C}, F_{21} = 0.00015 \text{ } ^\circ\text{C}^{-1}$$

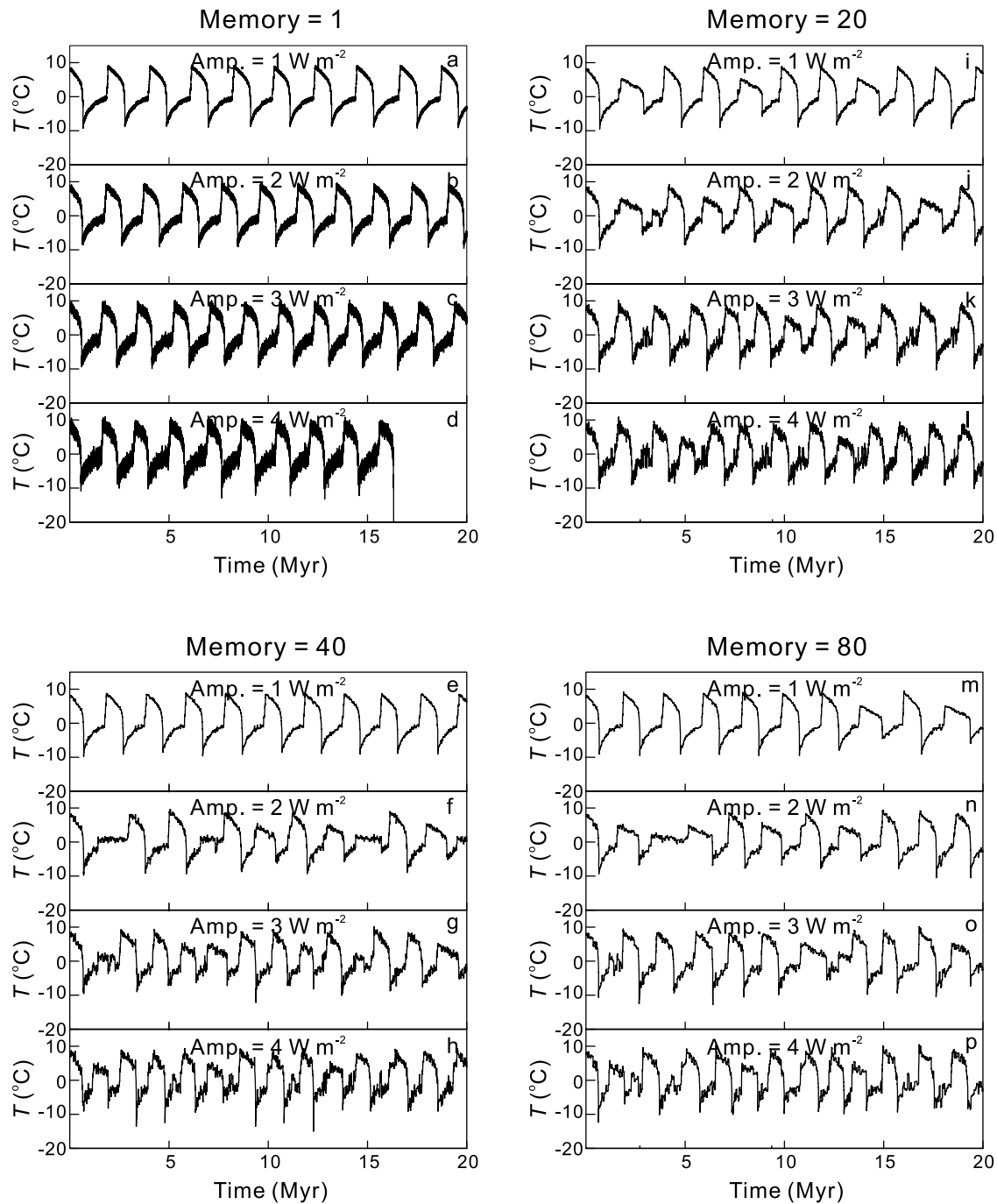


Figure 11. Time series of mean sea level temperature for runs in which the 570 Ma continental configuration is employed, but stochastic perturbations are applied. The memory of the perturbation in each set is the same and indicated on top of the set. The amplitude of the perturbation increases from the top to the bottom in each set.

stability of the system increases with the reference temperature. The critical amplitude of the perturbations quickly decreases to 3 W m^{-2} (Figure S11 of the auxiliary material) when the reference temperature is decreased to 1°C . Increasing the value of F_{21} to $0.0005^\circ\text{C}^{-1}$ again affects only

the period of the glacial oscillations (Figure S14 of the auxiliary material).

[48] Overall, for the same choice of the value of F_{21} , the climate for the 720 Ma continental configuration is found to be more vulnerable to stochastic perturbations than is climate for the 570 Ma continental configuration. The carbon

$$T_{\text{ref}} = 4 \text{ } ^\circ\text{C}, F_{21} = 0.00015 \text{ } ^\circ\text{C}^{-1}$$

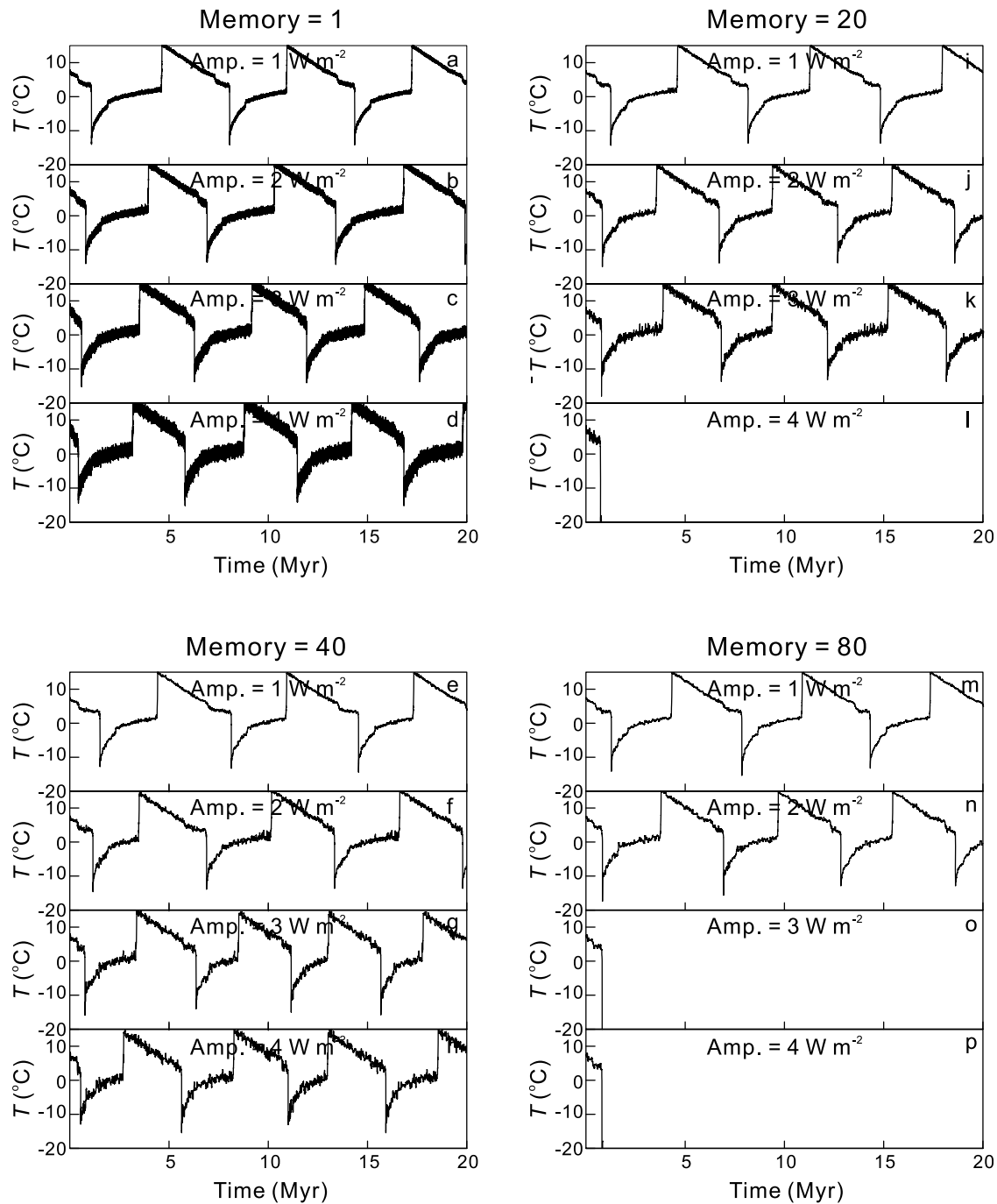


Figure 12. Similar to Figure 11 except that this is for the 720 Ma continental configuration.

cycle coupled climate system is also moderately sensitive to the reference temperature, the lower the reference temperature, the more susceptible the climate system to descent into a “hard snowball” state. It is important to understand that this parameter is poorly constrained. It would therefore be premature to assert that descent of the climate system into a “hard snowball” state for the equatorially centered supercontinent at 720 Ma was especially likely. The fact that a slight latitudinal shift of the 720 Ma continents can signif-

icantly improve the stability of the system also reinforces the view that the system may be rather stable.

3.3. Fit to the Observed $\delta^{13}\text{C}$ Data

[49] The variation of $\delta^{13}\text{C}$ in the inorganic reservoir is calculated for both the 570 Ma and 720 Ma models and compared with the observations in Figure 14. To be consistent with the equivalent analysis in the work of *Peltier et al.* [2007] for the 570 Ma model, the same values for β_{frac} and

$$T_{\text{ref}} = 4 \text{ } ^\circ\text{C}, F_{21} = 0.00015 \text{ } ^\circ\text{C}^{-1}$$

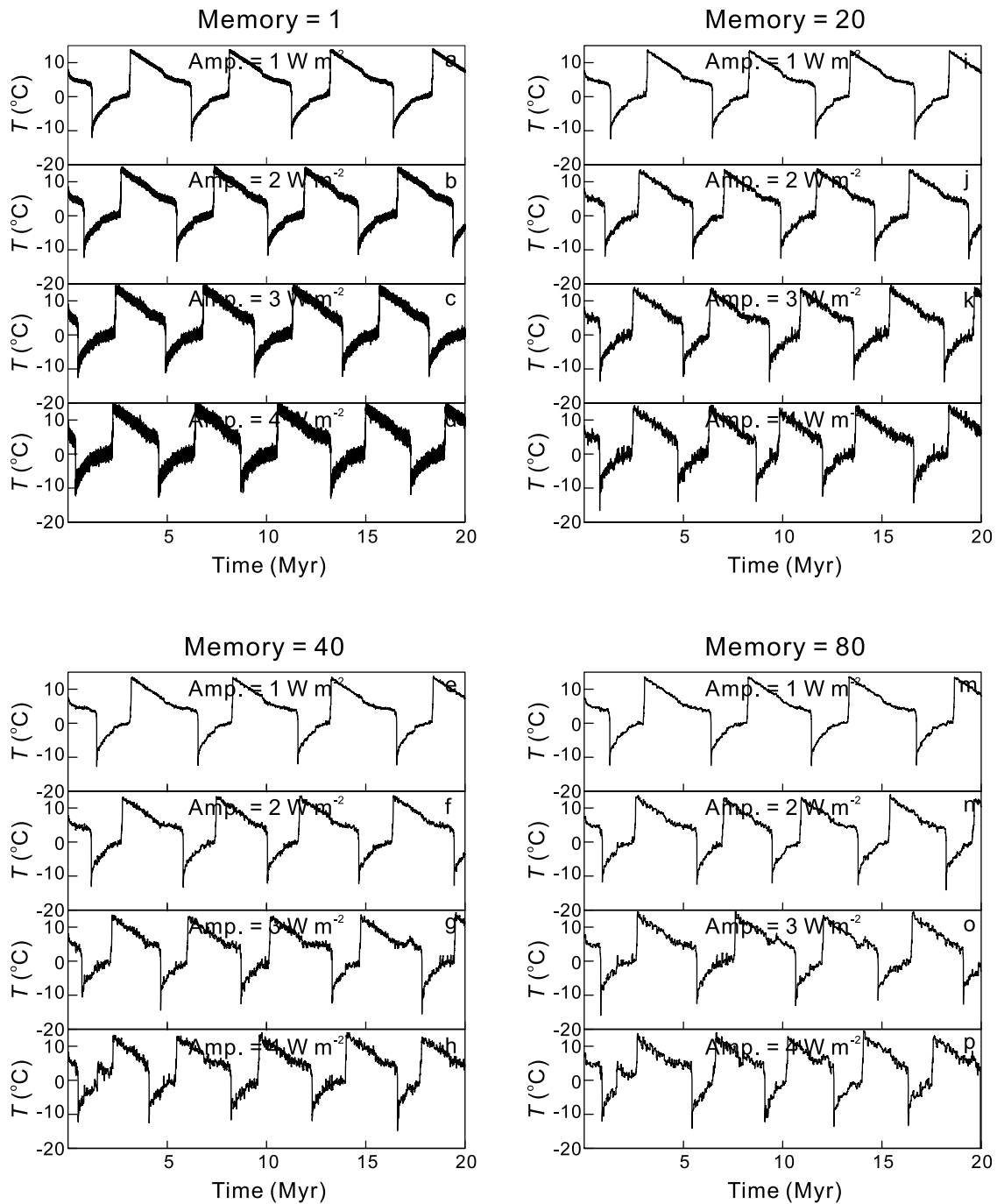


Figure 13. Similar to Figure 12 except that this is for the shifted 720 Ma geography.

ε_{0e} , i.e., 0.00048 per mil per gigaton and 28 per mil, respectively, are employed here to fit the observations. It is found that as the amplitude of the stochastic perturbations increases, the fit obtained to the data remains similar except that the maximum $\delta^{13}\text{C}$ of the model becomes slightly smaller. For the 720 Ma model, β_{frac} and ε_{0e} are set to 0.00014 per mil per gigaton and 24 per mil, respectively, in order to best fit the observations. The reason for this is that

the range of $p\text{CO}_2$ in the 720 Ma model is overall much higher than that in the 570 Ma model as can be inferred from the positions of the two solid lines in Figure 3. This is due to the significantly different geographies of the two models. The smaller value of β_{frac} for the 720 Ma model is consistent with that inferred for the Phanerozoic Eon (compare the slope of the thin solid line and that of the dashed line in Figure 3). Furthermore, the value of ε_{0e} for the 720 Ma

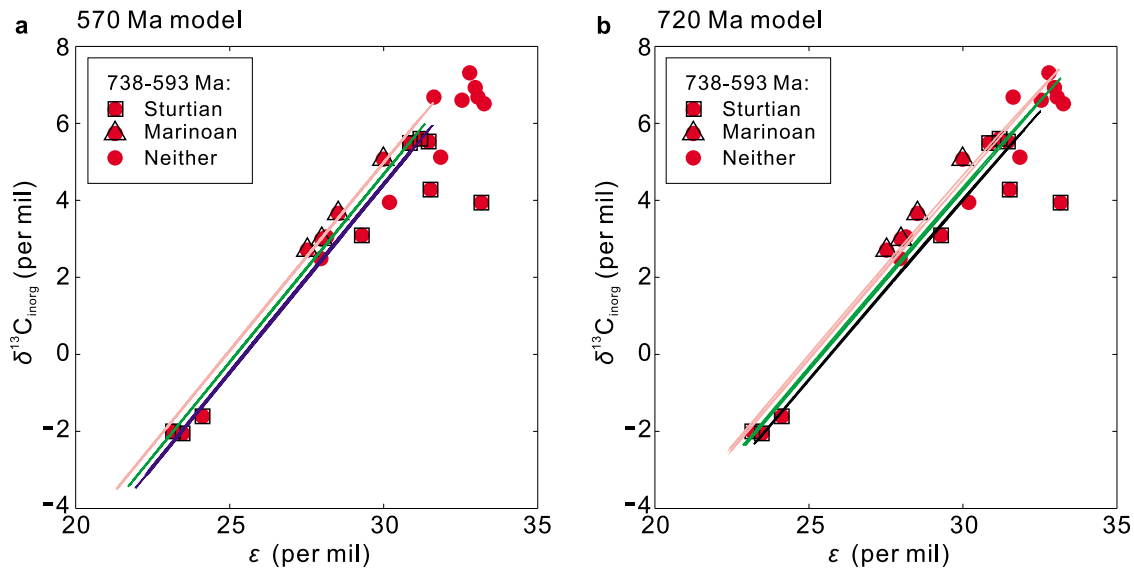


Figure 14. Variation of ^{13}C as a function of ϵ obtained from the (a) 570 Ma model and (b) 720 Ma model (employing the original 720 Ma geography), respectively, as compared to the observed data points during the period 738–593 Ma [Rothman *et al.*, 2003]. The pink, green, and blue lines are for the simulations with noise amplitude of 1 W m^{-2} , 2 W m^{-2} , and 3 W m^{-2} , respectively. The memories of the noise are all 20 time steps. Note that both the pink line and green line are shifted leftward slightly for clarity.

model, being smaller than that for 570 Ma, is also consistent with the values of ϵ_{toc} (essentially identical to ϵ_{0e} in this paper) in the work of Hayes *et al.* [1999, Figure 1]. The value of ϵ_{toc} in the work of Hayes *et al.* [1999] was obtained by directly analyzing similar data sets, so it is not surprising that ϵ_{0e} in our model is also constrained to a similar value even though it has been obtained by applying a completely different approach. Hayes *et al.* [1999] did not provide any definitive interpretation of the variations of ϵ_{toc} during the Neoproterozoic but pointed out that they might be associated with a change of the species of primary phytoplanktonic producers. The fact that the values of ϵ_{0e} and β_{frac} that have been used to fit the observations are both reasonable provides significant support for the reliability of both the carbon cycle model and the climate model components of the coupled structure we are employing.

[50] Although comparison of the model results with the available observational data has been successful, it would be unwarranted for us to claim that our model fully explains the carbon isotopic variations during late Neoproterozoic time. There were clearly other processes that would also have contributed to the variations of both $p\text{CO}_2$ and $\delta^{13}\text{C}$. For example, the release of methane from gas hydrates on the continental shelves and internal basin areas during the deglaciation could also have contributed to both climate warming and to shifting $\delta^{13}\text{C}$ to more negative values [Jiang *et al.*, 2003; Kennedy *et al.*, 2008; Wang *et al.*, 2008]. Moreover, the variation of the organic fraction of the carbon burial flux, f (see equation (10)), could also have contributed to some portion of the $\delta^{13}\text{C}$ variations, although this has been suggested not to be the primary cause [Rothman *et al.*, 2003]. Many other mechanisms for generating the negative $\delta^{13}\text{C}$ signals have also been proposed [e.g., Hoffman *et al.* [1998]; Higgins and Schrag [2003]]. Therefore the current model should rather be viewed as one emphasizing the

possible importance of the negative feedback mechanism that it embodies, one that further supports the plausibility of the “slushball” solutions as descriptions of late Neoproterozoic glacial extremes.

3.4. F_{21} , J_{21} , and the Strength of the Negative Feedback

[51] On the basis of inspection of equation (19), it seems clear that F_{21} is dependent solely on A , B , and $O_{2\text{sol,e}}$. It may be argued that since A and $O_{2\text{sol,e}}$ are relatively well known, and B has recently been measured based upon the oxidation rate of organic carbon in coal [Chang and Berner, 1999], the value of F_{21} is not as uncertain as has been suggested in this paper. However, it is important to note that there are processes other than direct oxidation of DOC that contribute to determining the appropriate value of B in equation (17). For example, the oxidation rate of DOC is not only determined by the solubility of oxygen in seawater but would also be influenced significantly by the upwelling of deep water which brings fresh DOC to the surface for oxidation. Another process that is not explicitly included in the model but which would effectively reduce the value of F_{21} is that some fraction of the CO_2 produced by enhanced remineralization may be reused in photosynthesis, a fertilization effect. Therefore the value of F_{21} remains very uncertain. A further contribution to the uncertainty concerning the value of F_{21} will be clear on the basis of equation (23). The strength of the negative feedback is there seen to be determined by the product of F_{21} and J_{21} .

3.5. Effect of Calcium-Magnesium Silicate Weathering

[52] On a long time scale, the major source of CO_2 is volcanic outgassing and the major sink is calcium-magnesium silicate weathering [e.g., Berner, 2004], silicate weathering therefore acting as a climate thermostat. As

climate cools, the weathering process slows down, a reaction that is further enhanced by the reduction of atmospheric precipitation and therefore of the runoff into the oceans. Where significant continental glaciation exists it may even be shut down completely if the runoff due to the calving of ice sheet ice into the oceans is negligible. This has led to the speculation in the “hard snowball” hypothesis [Hoffman and Schrag, 2000, 2002] that the apparent uniqueness of the Neoproterozoic glacial events might be due to the equatorial position of the continents, at least during the Sturtian episode. For such a continental configuration, climate cooling does not cause significant weakening of the weathering process because neither will the runoff decrease nor will the continents become ice covered so that the decrease of CO_2 continues and the cooling trend cannot be reversed or decreased in rate. A “hard snowball” state may result suddenly due to runaway ice-albedo feedback when the temperature of the climate is lowered below some critical point. The first half of this reasoning is logical on physical grounds and may well be the reason why the climate of the Late Neoproterozoic became so cold as to cause the onset of the Cryogenian interval. The second part of the hypothesis, however, is based on the assumption that there will be no intermediate state between a relatively warm state of climate and a “hard snowball” state. As demonstrated by Hyde *et al.* [2000] and Peltier *et al.* [2007] for the Marinoan continental configuration, and further by Liu and Peltier [2010] for the Sturtian configuration, before entering into a “hard snowball” state, the climate may first enter an intermediate “soft snowball” state. During the transition of the climate from a warm state into a “soft snowball” state, the continents are gradually covered by ice, starting from the polar edge of the continents, until the continents are completely ice covered by ice flow. Therefore the weathering process might be expected to be significantly weakened, acting as an efficient thermostat to reverse the cooling trend before descent into a “hard snowball” state can occur.

[53] It might also be argued, on the contrary, that the strength of silicate weathering would increase with increasing $p\text{CO}_2$ and could conceivably act to counter the effect of the negative feedback due to DOC remineralization. This idea is probably not viable insofar as “soft snowball” states are concerned, simply because the continents are almost completely ice covered during the time that CO_2 is being continuously released during the glacial phase of the cycle (Figure 6 here and Figure 5 in the work of Peltier *et al.* [2007]). On the basis of this argument, we have elected to assume that an exact balance exists between silicate weathering and volcanic outgassing in order to emphasize the importance of the negative feedback due to enhanced remineralization of DOC, in which case it is unnecessary to explicitly model the silicate weathering and volcanic outgassing processes.

[54] What we have done, rather, is to include the imbalance between silicate weathering and volcanic outgassing as one of the possible sources of stochastic perturbations. The initial motivation for this choice was that modeling the time dependence of volcanic outgassing would be entirely unconstrained. It might be imagined, however, that the imbalance between silicate weathering and volcanic outgassing is mainly caused by the variation of the rate of the former associated with the variation of $p\text{CO}_2$ and thus cli-

mate. In this case the imbalance could not reasonably be treated as stochastic noise but rather would be predictable if the silicate weathering were explicitly parameterized in the model as a function of climate state. It is true that this source of imbalance is not stochastic if the volcanic activity is known but, as argued above, in the “soft snowball” regime, the silicate weathering is almost independent of the variation of atmospheric CO_2 . In fact, on the timescale of the “soft snowball” glacial cycle, the variation of silicate weathering associated with the variation of land ice cover is much more significant, and it acts in the same direction as the negative feedback mechanism due to DOC remineralization so as to prevent the occurrence of a “hard snowball” state. Including this process in the model explicitly would only obscure the role of the negative feedback associated with DOC remineralization. We are more interested in the stochastic part of the imbalance associated with volcanic activity because this part of the imbalance can act either to prevent or to promote “hard snowball” formation. The focus of this paper has been upon testing the ability of the climate system to resist descent into the hard snowball state due to the occurrence of adverse perturbations.

3.6. Oxygen Availability and the Oxygen Requirement

[55] The availability of sufficient atmospheric oxygen is clearly critical to operation of the mechanism proposed by Peltier *et al.* [2007] as a control on Neoproterozoic glaciation. The level of O_2 in the atmosphere had probably risen to at least 0.02–0.04 atmospheric pressure (1 atm) at the beginning of the Neoproterozoic Era (~1000 Ma) [Cailing and Zahnle, 2003; Holland, 2006; Kasting, 1993], and to a substantially higher level by the late Neoproterozoic period [Canfield *et al.*, 2007; Fike *et al.*, 2006; Holland, 2006; McFadden *et al.*, 2008; Scott *et al.*, 2008]. Although the ubiquitous oxygenation of the deep ocean is inferred not to have occurred until after the Gaskiers glaciation (~580 Ma) [Canfield *et al.*, 2007; McFadden *et al.*, 2008], the O_2 concentration in the atmosphere and the surface ocean could have increased well before the Gaskiers glaciation. For example, the earlier oxidation of the atmosphere and surface ocean prior to that of the deep ocean has been inferred to have been the case for the Great Oxidation Event of the early Paleoproterozoic [Anbar *et al.*, 2007; Farquhar *et al.*, 2000; Kaufman *et al.*, 2007]. Therefore the concentration of atmospheric O_2 would most probably have reached a much higher level than 0.04 atm well before the Sturtian glaciation (~720 Ma). However, even if the O_2 level of 0.04 atm is assumed to have existed just prior to the Sturtian glaciation, the simple calculation below will show that even this would have been sufficient for the remineralization process to produce the CO_2 required to warm the planet from a slushball state.

[56] In equation (25), $p\text{CO}_{2e}$ is assumed to be equal to 300 ppmv. To warm the planet from a “soft snowball” state, $p\text{CO}_2$ needs to be increased to around 500 ppmv, so the mass (M_1) of the DIC reservoir should increase by a factor of 1.29 relative to its equilibrium value, for which we have used the modern mass of 40000 gigatons. The change of M_1 is then $\Delta M_1 = 0.29 * M_1$, which if expressed in moles of CO_2 is 2.6×10^{14} moles, which is also the same number of moles of O_2 required to remineralize DOC. However, the number of moles of O_2 in the atmosphere was 6.5×10^{18} even when

the O_2 level was only 0.04 atm, 4 orders of magnitude larger than required. Even if we consider the extreme case in which the efficiency of utilization of the dissolved O_2 in the remineralization process was only 5% (meaning that 20 times more O_2 was needed to be dissolved in ocean water) and 3000 ppmv of pCO_2 was required to warm the planet, the total amount of O_2 required to be taken up from the atmosphere was 1.1×10^{16} moles, less than 1% of the O_2 that was available. Therefore the O_2 level during the late Neoproterozoic period was not a limitation on the reasonableness of the proposed mechanism.

3.7. Individual Glacial Events and Glacial Cycles Predicted by the Model

[57] Three potentially global glaciations are inferred to have occurred during the Neoproterozoic, the Sturtian, Marinoan, and Gaskiers glaciations. Each of these events is inferred to have been separated by ~ 70 Myrs. It therefore follows that if the timing of the events is reliable and the three events were connected, for example through the operation of the carbon cycle, this would imply that the glacial cycles were of extremely long duration of approximately 70 Myrs. This possibility is questionable and has been questioned. During both the glacial and interglacial phases of these previously inferred global glacial events, episodes with periods of order 1–5 Myr have been interpreted on the basis of sedimentology to reveal the continuous existence of an active hydrological cycle [Rieu *et al.*, 2007]. Allen and Etienne [2008] then continue to question the global correlations of glacial events due to uncertainties in the age measurements and argue that ~ 5 glacial events might have occurred between 780–630 Ma. This would then imply a period of 30 Myr for the glacial cycles. The model we have developed is able to produce this full range of periods by appropriate adjustment of the strength of the feedback process, which is currently poorly constrained by observations. As discussed by Peltier *et al.* [2007], the strength of the feedback process is controlled by the parameter F_{21} , decreasing which can extend the period of the cycles from ~ 1 Myr to many 10s of Myrs. Including the stochastic perturbations in the model further complicates the nature of the cyclicity predicted. As demonstrated in Figure 11, the amplitude of the temperature oscillations is sometimes smaller and the timescale shorter. Whether or not the shorter timescale oscillations delivered by the model might be representative of the short timescale (1–5 Myr) variability inferred to have occurred by Rieu *et al.* [2007], and the larger amplitude primary oscillations be representative of the glacial cycles discussed by Allen and Etienne [2008] remains an open question.

[58] Whether the multiple glaciations of the Neoproterozoic might be represented as multiple circuits of the same hysteresis loop is also unclear, however, as the nature of the hysteresis loop has been shown to be a strong function of continental configuration. It may well be, on the contrary, that the individual Neoproterozoic glacial events are better understood as isolated circuits of the different hysteresis loops that were characteristic of the system during the Sturtian, Marinoan, and Gaskiers epochs. These individual glacial cycles would then, upon termination, leave the system in a state such that appropriate initial conditions would have to be reestablished before a new carbon cycle mediated

ice age cycle could occur. This is especially true if the glacial ocean was not saturated with respect to carbonate so that the atmospheric pCO_2 increased to a very high value after the termination of a “soft snowball” due the remineralization of DOC.

4. Conclusions

[59] It has been demonstrated that the model in the work of Peltier *et al.* [2007] is robust against the introduction of different continental configurations that may be more appropriate to that characteristic of the Sturtian glaciation [Liu and Peltier, 2010]. Herein we have further demonstrated that the robustness of the cyclic glaciation process supported by the model persists in the presence of both orbital perturbations and large amplitude stochastic perturbations. However, the cyclicity itself is sensitive not only to continental configuration but also to the specific choice of the parameters F_{21} and reference temperature. The origin of the stochastic perturbations we have explicitly considered could be associated with the imbalance between the volcanic outgassing source of atmospheric pCO_2 and the calcium-magnesium silicate weathering sink. This component of the forcing is also intended to encompass a much broader range of additional physical processes not explicitly discussed in the model. If the value of F_{21} is as small as $0.00015^\circ C^{-1}$, and the reference temperature is $4^\circ C$ for the 720 Ma continental configuration and $0^\circ C$ for the 570 Ma continental configuration, we have inferred the climate state to be more stable for the 570 Ma continental configuration than for the 720 Ma configuration. The more recent surface configuration of the continents remains in the “soft snowball” regime under stochastic perturbations of amplitude as high as $4 W m^{-2}$ (Figure 11), which is equivalent to a perturbation which halves or doubles atmospheric pCO_2 . On the other hand, the earlier configuration can be kicked out of the “soft snowball” regime into a “hard snowball” state by stochastic perturbations of $3 W m^{-2}$ (Figure 12), corresponding to a variation of pCO_2 of only 60%. However, a slight shift of the 720 Ma configuration by 5° toward the South Pole, which is well within the uncertainties in the paleomagnetic reconstruction, greatly improves the stability of the climate against perturbations (again up to $4 W m^{-2}$, Figure 13). Moreover, although this has not been tested explicitly, it can be inferred from Figures 8–10 that the climate will be more stable when the reference temperature is higher and more stable if the value of F_{21} is further reduced.

[60] Of course, the primary issue remains outstanding as to whether the actual ice sheet coupled climate system possesses the hysteresis embodied in the simple model that has been the focus of analysis in this paper and that of Liu and Peltier [2010]. Although an early attempt by Peltier *et al.* [2004], based upon analyses performed using a detailed coupled atmosphere-ocean model, the NCAR CSM1.4 model, suggested that such structure could exist, this issue must be considered to remain open and will be the target of further analyses to be described elsewhere.

[61] **Acknowledgments.** This paper is a contribution to the work of the Polar Climate Stability Network that is funded by the Canadian Foundation for Climate and Atmospheric Science and a consortium of Canadian Universities. Further support was provided by NSERC Discovery grant

A9627. The required computations were performed on the SciNet facility at the University of Toronto which is a component of the Compute Canada HPC platform. We are indebted to the referees for guiding us to the work of Zeebe and Wolf-Gladrow [2001] which has helped us to better understand the detailed characteristics of the ocean carbon cycle.

References

- Allen, P. A., and J. L. Etienne (2008), Sedimentary challenge to Snowball Earth, *Nat. Geosci.*, *1*(12), 817–825, doi:10.1038/ngeo355.
- Allen, P. A., J. Leather, and M. D. Brasier (2004), The Neoproterozoic Fiq glaciation and its aftermath, Huqf supergroup of Oman, *Basin Res.*, *16*(4), 507–534, doi:10.1111/j.1365-2117.2004.00249.x.
- Anbar, A. D., et al. (2007), A whiff of oxygen before the Great Oxidation Event?, *Science*, *317*(5846), 1903–1906, doi:10.1126/science.1140325.
- Anderson, S. P. (2007), Biogeochemistry of glacial landscape systems, *Annu. Rev. Earth Planet. Sci.*, *35*, 375–399, doi:10.1146/annurev.earth.35.031306.140033.
- Berner, R. A. (2004), *The Phanerozoic Carbon Cycle: CO₂ and O₂*, 150 pp., Oxford Univ. Press, Oxford, U. K.
- Canfield, D. E., S. W. Poulton, and G. M. Narbonne (2007), Late-Neoproterozoic deep-ocean oxygenation and the rise of animal life, *Science*, *315*(5808), 92–95, doi:10.1126/science.1135013.
- Canfield, D. E., S. W. Poulton, A. H. Knoll, G. M. Narbonne, G. Ross, T. Goldberg, and H. Strauss (2008), Ferruginous conditions dominated later neoproterozoic deep-water chemistry, *Science*, *321*(5891), 949–952, doi:10.1126/science.1154499.
- Catling, D., and K. Zahnle (2003), Evolution of atmospheric oxygen, in *Encyclopedia of Atmospheric Sciences*, edited by J. R. Holton, J. A. Curry, and J. A. Pyle, pp. 754–761, Academic, San Diego, Calif., doi:10.1016/B0-12-227090-8/00291-8.
- Chandler, M. A., and L. E. Sohl (2000), Climate forcings and the initiation of low-latitude ice sheets during the Neoproterozoic Varanger glacial interval, *J. Geophys. Res.*, *105*(D16), 20,737–20,756, doi:10.1029/2000JD900221.
- Chang, S. B., and R. A. Berner (1999), Coal weathering and the geochemical carbon cycle, *Geochim. Cosmochim. Acta*, *63*(19–20), 3301–3310, doi:10.1016/S0016-7037(99)00252-5.
- Church, M. J. (2008), Resource control of bacterial dynamics in the sea, in *Microbial Ecology of the Oceans*, edited by D. L. Kirchman, pp. 335–382, John Wiley, Hoboken, N. J., doi:10.1002/9780470281840.ch10.
- Condon, D., M. Zhu, S. Bowring, W. Wang, A. Yang, and Y. Jin (2005), U-Pb ages from the neoproterozoic Doushantuo Formation, China, *Science*, *308*(5718), 95–98, doi:10.1126/science.1107765.
- Crowley, T. J., W. T. Hyde, and W. R. Peltier (2001), CO₂ levels required for deglaciation of a “Near-Snowball” Earth, *Geophys. Res. Lett.*, *28*(2), 283–286, doi:10.1029/2000GL011836.
- DeBlonde, G., and W. R. Peltier (1990), A model of late Pleistocene ice sheet growth with realistic geography and simplified cryodynamics and geodynamics, *Clim. Dyn.*, *5*(2), 103–110, doi:10.1007/BF00207425.
- DeBlonde, G., and W. R. Peltier (1991), Simulations of continental ice sheet growth over the last glacial-interglacial cycle: Experiments with a one-level seasonal energy balance model including realistic geography, *J. Geophys. Res.*, *96*(D5), 9189–9215, doi:10.1029/90JD02606.
- DeBlonde, G., and W. R. Peltier (1993), Late Pleistocene ice-age scenarios based on observational evidence, *J. Clim.*, *6*(4), 709–727, doi:10.1175/1520-0442(1993)006<0709:LPIASB>2.0.CO;2.
- DeBlonde, G., W. R. Peltier, and W. T. Hyde (1992), Simulations of continental ice sheet growth over the last glacial-interglacial cycle: Experiments with a one level seasonal energy balance model including seasonal ice albedo feedback, *Palaeogeogr. Palaeoclimatol. Paleocol.*, *98*(1), 37–55, doi:10.1016/0031-0182(92)90255-4.
- Donnadieu, Y., Y. Godd ris, G. Ramstein, A. N d lec, and J. Meert (2004), A ‘snowball Earth’ climate triggered by continental break-up through changes in runoff, *Nature*, *428*(6980), 303–306, doi:10.1038/nature02408.
- Ducklow, H. W. (2003), Biogeochemical provinces: Towards a JGOFS synthesis, in *Ocean Biogeochemistry: The Role of the Ocean Carbon Cycle in Global Change*, edited by M. J. R. Fasham, pp. 3–17, Springer, Berlin.
- Evans, D. A. D. (2006), Proterozoic low orbital obliquity and axial-dipolar geomagnetic field from evaporite palaeolatitudes, *Nature*, *444*(7115), 51–55, doi:10.1038/nature05203.
- Farquhar, J., H. M. Bao, and M. Thiemens (2000), Atmospheric influence of Earth’s earliest sulfur cycle, *Science*, *289*(5480), 756–758, doi:10.1126/science.289.5480.756.
- Fike, D. A., J. P. Grotzinger, L. M. Pratt, and R. E. Summons (2006), Oxidation of the Ediacaran Ocean, *Nature*, *444*(7120), 744–747, doi:10.1038/nature05345.
- Font, E., R. I. F. Trindade, and A. N d lec (2005), Detrital remanent magnetization in haematite-bearing Neoproterozoic Puga cap dolostone, Amazon craton: A rock magnetic and SEM study, *Geophys. J. Int.*, *163*(2), 491–500, doi:10.1111/j.1365-246X.2005.02776.x.
- Garcia, H. E., and L. I. Gordon (1992), Oxygen solubility in seawater – Better fitting equations, *Limnol. Oceanogr.*, *37*(6), 1307–1312, doi:10.4319/lo.1992.37.6.1307.
- Gibbs, M. T., and L. R. Kump (1994), Global chemical erosion during the Last Glacial Maximum and the present – Sensitivity to changes in lithology and hydrology, *Paleoceanography*, *9*(4), 529–543, doi:10.1029/94PA01009.
- Gislason, S. R., E. H. Oelkers, and A. Snorrason (2006), Role of river-suspended material in the global carbon cycle, *Geology*, *34*(1), 49–52, doi:10.1130/G22045.1.
- Godd ris, Y., and Y. Donnadieu (2008), Carbon cycling and snowball Earth, *Nature*, *456*(7224), 9–10.
- Gough, D. O. (1981), Solar interior structure and luminosity variations, *Sol. Phys.*, *74*(1), 21–34, doi:10.1007/BF00151270.
- Hayes, J. M., H. Strauss, and A. J. Kaufman (1999), The abundance of C-13 in marine organic matter and isotopic fractionation in the global biogeochemical cycle of carbon during the past 800 Ma, *Chem. Geol.*, *161*(1–3), 103–125, doi:10.1016/S0009-2541(99)00083-2.
- Higgins, J. A., and D. P. Schrag (2003), Aftermath of a snowball Earth, *Geochim. Geophys. Syst.*, *4*(3), 1028, doi:10.1029/2002GC000403.
- Hoffman, P. F., and D. P. Schrag (2000), Snowball earth, *Sci. Am.*, *282*(1), 68–75, doi:10.1038/scientificamerican0100-68.
- Hoffman, P. F., and D. P. Schrag (2002), The snowball Earth hypothesis: Testing the limits of global change, *Terra Nova*, *14*(3), 129–155, doi:10.1046/j.1365-3121.2002.00408.x.
- Hoffman, P. F., A. J. Kaufman, G. P. Halverson, and D. P. Schrag (1998), A Neoproterozoic snowball earth, *Science*, *281*(5381), 1342–1346, doi:10.1126/science.281.5381.1342.
- Hoffman, P. F., J. W. Crowley, D. T. Johnston, D. S. Jones, and D. P. Schrag (2008), Snowball prevention questioned, *Nature*, *456*(7224), 9–10, doi:10.1038/nature07655.
- Holland, H. D. (2006), The oxygenation of the atmosphere and oceans, *Phil. Trans. R. Soc. London, Ser. B*, *361*(1470), 903–915, doi:10.1098/rstb.2006.1838.
- Hyde, W. T., T. J. Crowley, S. K. Baum, and W. R. Peltier (2000), Neoproterozoic ‘snowball Earth’ simulations with a coupled climate/ice-sheet model, *Nature*, *405*(6785), 425–429, doi:10.1038/35013005.
- Jiang, G. Q., M. J. Kennedy, and N. Christie-Blick (2003), Stable isotopic evidence for methane seeps in Neoproterozoic postglacial cap carbonates, *Nature*, *426*(6968), 822–826, doi:10.1038/nature02201.
- Joint, I., P. Henriksen, G. A. Fones, D. Bourne, T. F. Thingstad, and B. Riemann (2002), Competition for inorganic nutrients between phytoplankton and bacterioplankton in nutrient manipulated mesocosms, *Aquat. Microb. Ecol.*, *29*(2), 145–159, doi:10.3354/ame029145.
- Kasting, J. F. (1993), Earths Early Atmosphere, *Science*, *259*(5097), 920–926, doi:10.1126/science.11536547.
- Kaufman, A. J., D. T. Johnston, J. Farquhar, A. L. Masterson, T. W. Lyons, S. Bates, A. D. Anbar, G. L. Arnold, J. Garvin, and R. Buick (2007), Late Archean biospheric oxygenation and atmospheric evolution, *Science*, *317*(5846), 1900–1903, doi:10.1126/science.1138700.
- Kennedy, M., D. Mrofka, and C. von der Borch (2008), Snowball Earth termination by destabilization of equatorial permafrost methane clathrate, *Nature*, *453*(7195), 642–645, doi:10.1038/nature06961.
- Kirschvink, J. L. (1992), Late Proterozoic low latitude glaciation: The snowball Earth, in *The Proterozoic Biosphere: A Multi-Disciplinary Study*, edited by J. W. Schopf and C. Klein, pp. 51–52, Cambridge Univ. Press, Cambridge, U. K.
- Kump, L. R., and M. A. Arthur (1999), Interpreting carbon-isotope excursions: Carbonates and organic matter, *Chem. Geol.*, *161*(1–3), 181–198, doi:10.1016/S0009-2541(99)00086-8.
- Le Guerrou , E., P. A. Allen, and A. Cozzi (2006), Chemostratigraphic and sedimentological framework of the largest negative carbon isotopic excursion in Earth history: The Neoproterozoic Shuram. Formation (Nafun Group, Oman), *Precambrian Res.*, *146*(1–2), 68–92, doi:10.1016/j.precamres.2006.01.007.
- Le Hir, G., G. Ramstein, Y. Donnadieu, and R. T. Pierrehumbert (2007), Investigating plausible mechanisms to trigger a deglaciation from a hard snowball Earth, *C. R. Geosci.*, *339*(3–4), 274–287, doi:10.1016/j.crte.2006.09.002.
- Leather, J., P. A. Allen, M. D. Brasier, and A. Cozzi (2002), Neoproterozoic snowball earth under scrutiny: Evidence from the Fiq glaciation of Oman, *Geology*, *30*(10), 891–894, doi:10.1130/0091-7613(2002)030<0891:NSEUSE>2.0.CO;2.
- Li, Z. X. (2000), New palaeomagnetic results from the ‘cap dolomite’ of the Neoproterozoic Walsh Tillite, northwestern Australia, *Precambrian Res.*, *100*(1–3), 359–370, doi:10.1016/S0301-9268(99)00081-9.

- Li, Z. X., D. A. D. Evans, and S. Zhang (2004), A 90 degrees spin on Rodinia: Possible causal links between the Neoproterozoic supercontinent, superplume, true polar wander and low-latitude glaciation, *Earth Planet. Sci. Lett.*, 220(3–4), 409–421, doi:10.1016/S0012-821X(04)00064-0.
- Li, Z. X., et al. (2008), Assembly, configuration, and break-up history of Rodinia: A synthesis, *Precambrian Res.*, 160(1–2), 179–210, doi:10.1016/j.precamres.2007.04.021.
- Liu, Y., and W. R. Peltier (2010), A carbon cycle coupled climate model of Neoproterozoic glaciation: Influence of continental configuration on the formation of a “soft snowball,” *J. Geophys. Res.*, 115, D17111, doi:10.1029/2009JD013082.
- McFadden, K. A., J. Huang, X. L. Chu, G. Q. Jiang, A. J. Kaufman, C. M. Zhou, X. L. Yuan, and S. H. Xiao (2008), Pulsed oxidation and biological evolution in the Ediacaran Doushantuo Formation, *Proc. Natl. Acad. Sci. U. S. A.*, 105(9), 3197–3202, doi:10.1073/pnas.0708336105.
- Munhoven, G., and L. M. Francois (1994), Glacial-interglacial changes in continental weathering: Possible implications for atmospheric CO₂, in *Carbon Cycling in the Glacial Ocean: Constraints on the Ocean's Role in Global Change*, edited by R. Zahn et al., pp. 39–60, Springer, Berlin.
- Myhre, G., and F. Stordal (1997), Role of spatial and temporal variations in the computation of radiative forcing and GWP, *J. Geophys. Res.*, 102(D10), 11,181–11,200, doi:10.1029/97JD00148.
- Myhre, G., E. J. Highwood, K. P. Shine, and F. Stordal (1998), New estimates of radiative forcing due to well mixed greenhouse gases, *Geophys. Res. Lett.*, 25(14), 2715–2718, doi:10.1029/98GL01908.
- Nagata, T. (2008), Organic matter–bacteria interactions in seawater, in *Microbial Ecology of the Oceans*, edited by D. L. Kirchman, pp. 207–241, John Wiley, Hoboken, N. J., doi:10.1002/9780470281840.ch7.
- North, G. R., R. F. Cahalan, and J. A. Coakley (1981), Energy-balance climate models, *Rev. Geophys.*, 19(1), 91–121, doi:10.1029/RG019i001p00091.
- Peltier, W. R., and Y. G. Liu (2008), Carbon cycling and snowball Earth Reply, *Nature*, 456(7224), E9–E10, doi:10.1038/nature07656.
- Peltier, W. R., L. Tarasov, G. Vettoretti, and L. P. Solheim (2004), Climate dynamics in deep time: Modeling the “snowball bifurcation” and assessing the plausibility of its occurrence, in *The Extreme Proterozoic: Geology, Geochemistry and Climate*, edited by G. S. Jenkins et al., pp. 107–124, AGU, Washington, DC.
- Peltier, W. R., Y. G. Liu, and J. W. Crowley (2007), Snowball Earth prevention by dissolved organic carbon remineralization, *Nature*, 450(7171), 813–818, doi:10.1038/nature06354.
- Pierrehumbert, R. T. (2004), High levels of atmospheric carbon dioxide necessary for the termination of global glaciation, *Nature*, 429(6992), 646–649, doi:10.1038/nature02640.
- Pierrehumbert, R. T. (2005), Climate dynamics of a hard snowball Earth, *J. Geophys. Res.*, 110, D01111, doi:10.1029/2004JD005162.
- Poulsen, C. J. (2003), Absence of a runaway ice-albedo feedback in the Neoproterozoic, *Geology*, 31(6), 473–476, doi:10.1130/0091-7613(2003)031<0473:AOARIF>2.0.CO;2.
- Poulsen, C. J., and R. L. Jacob (2004), Factors that inhibit snowball Earth simulation, *Paleoceanography*, 19, PA4021, doi:10.1029/2004PA001056.
- Ramanathan, V., M. S. Lian, and R. D. Cess (1979), Increased atmospheric CO₂: Zonal and seasonal estimates of the effect on the radiation energy balance and surface temperature, *J. Geophys. Res.*, 84(C8), 4949–4958, doi:10.1029/JC084iC08p04949.
- Ridgwell, A. J., M. J. Kennedy, and K. Caldeira (2003), Carbonate deposition, climate stability, and neoproterozoic ice ages, *Science*, 302(5646), 859–862, doi:10.1126/science.1088342.
- Rieu, R., P. A. Allen, M. Plotze, and T. Pettke (2007), Climatic cycles during a Neoproterozoic “snowball” glacial epoch, *Geology*, 35(4), 299–302, doi:10.1130/G23400A.1.
- Robinson, C. (2008), Heterotrophic bacterial respiration, in *Microbial Ecology of the Ocean*, edited by D. L. Kirchman, pp. 299–334, John Wiley, Hoboken, N. J., doi:10.1002/9780470281840.ch9.
- Rothman, D. H., J. M. Hayes, and R. E. Summons (2003), Dynamics of the Neoproterozoic carbon cycle, *Proc. Natl. Acad. Sci. U. S. A.*, 100(14), 8124–8129, doi:10.1073/pnas.0832439100.
- Schrag, D. P., and P. F. Hoffman (2001), Geophysics - Life, geology and snowball Earth, *Nature*, 409(6818), 306, doi:10.1038/35053170.
- Scott, C., T. W. Lyons, A. Bekker, Y. Shen, S. W. Poulton, X. Chu, and A. D. Anbar (2008), Tracing the stepwise oxygenation of the Proterozoic ocean, *Nature*, 452(7186), 456–459, doi:10.1038/nature06811.
- Shackleton, N. J., A. Berger, and W. R. Peltier (1990), An alternative astronomical calibration of the Lower Pleistocene timescale based on ODP Site 677, *Trans. R. Soc. Edinburgh Earth Sci.*, 81, 251–261.
- Sigman, D. M., M. P. Hain, and G. H. Haug (2010), The polar ocean and glacial cycles in atmospheric CO₂ concentration, *Nature*, 466(7302), 47–55, doi:10.1038/nature09149.
- Sohl, L. E., N. Christie-Blick, and D. V. Kent (1999), Paleomagnetic polarity reversals in Marinoan (ca. 600 Ma) glacial deposits of Australia: Implications for the duration of low-latitude glaciation in neoproterozoic time, *Geol. Soc. Am. Bull.*, 111(8), 1120–1139, doi:10.1130/0016-7606(1999)111<1120:PPRIMC>2.3.CO;2.
- Stastna, M., and W. R. Peltier (2007), On box models of the North Atlantic thermohaline circulation: Intrinsic and extrinsic millennial timescale variability in response to deterministic and stochastic forcing, *J. Geophys. Res.*, 112, C10023, doi:10.1029/2006JC003938.
- Stefánsdóttir, M. B., and S. R. Gislason (2005), The erosion and suspended matter/seawater interaction during and after the 1996 outburst flood from the Vatnajökull Glacier, Iceland, *Earth Planet. Sci. Lett.*, 237(3–4), 433–452, doi:10.1016/j.epsl.2005.07.002.
- Tarasov, L., and W. R. Peltier (1997), Terminating the 100 kyr ice age cycle, *J. Geophys. Res.*, 102(D18), 21,665–21,693, doi:10.1029/97JD01766.
- Tarasov, L., and W. R. Peltier (1999), Impact of thermomechanical ice sheet coupling on a model of the 100 kyr ice age cycle, *J. Geophys. Res.*, 104(D8), 9517–9545, doi:10.1029/1998JD200120.
- Tarasov, L., and W. R. Peltier (2002), Greenland glacial history and local geodynamic consequences, *Geophys. J. Int.*, 150(1), 198–229, doi:10.1046/j.1365-246X.2002.01702.x.
- Tarasov, L., and W. R. Peltier (2003), Greenland glacial history, borehole constraints, and Eemian extent, *J. Geophys. Res.*, 108(B3), 2143, doi:10.1029/2001JB001731.
- Tranter, M., P. Huybrechts, G. Munhoven, M. J. Sharp, G. H. Brown, I. W. Jones, A. J. Hodson, R. Hodgkins, and J. L. Wadham (2002), Direct effect of ice sheets on terrestrial bicarbonate, sulphate and base cation fluxes during the last glacial cycle: Minimal impact on atmospheric CO₂ concentrations, *Chem. Geol.*, 190(1–4), 33–44, doi:10.1016/S0009-2541(02)00109-2.
- Trindade, R. I. F., and M. Macouin (2007), Palaeolatitudes of glacial deposits and palaeogeography of Neoproterozoic ice ages, *C. R. Geosci.*, 339(3–4), 200–211, doi:10.1016/j.crte.2007.02.006.
- Wang, J. S., G. Q. Jiang, S. H. Xiao, Q. Li, and Q. Wei (2008), Carbon isotope evidence for widespread methane seeps in the ca. 635 Ma Doushantuo cap carbonate in south China, *Geology*, 36(5), 347–350, doi:10.1130/G24513A.1.
- Zeebe, R. E., and D. A. Wolf-Gladrow (2001), *CO₂ in Seawater: Equilibrium, Kinetics, Isotopes*, Elsevier, Amsterdam.

Y. Liu and W. R. Peltier, Department of Physics, University of Toronto, 60 St. George Street, Toronto, ON M5S 1A7, Canada. (ygliu@atmosph.physics.utoronto.ca)